

**AN ANALYSIS OF DEFORMATION BEHAVIOR OF MURATLI ASPHALT
FACED ROCKFILL DAM**

**A THESIS SUBMITTED TO
THE GRADUATE SCHOOL OF NATURAL AND APPLIED SCIENCES
OF
MIDDLE EAST TECHNICAL UNIVERSITY**

BY

YEŞİM SEMA ÜNSEVER

**IN PARTIAL FULFILLMENT OF THE REQUIREMENTS
FOR
THE DEGREE OF MASTER OF SCIENCE
IN
CIVIL ENGINEERING**

JULY 2007

Approval of the Thesis

**“AN ANALYSIS OF DEFORMATION BEHAVIOR OF MURATLI ASPHALT
FACED ROCKFILL DAM”**

Submitted by **YEŞİM SEMA ÜNSEVER** in partial fulfillment of the requirements
for the degree of **Master of Science in Civil Engineering** by,

Prof. Dr. Canan Özgen
Dean, Graduate School of **Natural and Applied Sciences** _____

Prof. Dr. Güney Özcebe
Head of Department, **Civil Engineering** _____

Prof. Dr. M. Yener Özkan
Supervisor, **Civil Engineering, METU** _____

Gülru S. Yıldız
Co-supervisor, **State Hydraulic Works** _____

Examining Committee Members:

Prof. Dr. Ufuk Ergun (*)
Civil Engineering, METU _____

Prof. Dr. M. Yener Özkan (**)
Civil Engineering, METU _____

Assoc. Prof. Dr. K. Önder Çetin
Civil Engineering, METU _____

Dr. Serap Cılız
MİTAŞ _____

Gülru S. Yıldız
State Hydraulic Works _____

Date: _____ 20.07.2007

(*) Head of Examining Committee

(**) Supervisor

I hereby declare that all information in this document has been obtained and presented in accordance with academic rules and ethical conduct. I also declare that, as required by these rules and conduct, I have fully cited and referenced all material and results that are not original to this work.

Name, Last name : Yeşim Sema ÜNSEVER

Signature :

ABSTRACT

AN ANALYSIS OF DEFORMATION BEHAVIOR OF MURATLI ASPHALT FACED ROCKFILL DAM

ÜNSEVER, Yeşim Sema

M.S., Department of Civil Engineering

Supervisor : Prof. Dr. M. Yener ÖZKAN

Co-Supervisor: Gülru S. YILDIZ

July 2007, 96 Pages

In this study, settlement and seepage behavior of Muratlı Dam, which is the first asphalt faced rockfill dam in Turkey, is investigated for the “end of construction” and “reservoir impoundment” loading conditions. Two dimensional plane strain finite element analyses are carried out in order to determine the total stresses, displacements and pore water pressures. Hardening soil model is used in order to represent the non-linear, inelastic and stress dependent behavior of rockfill material. Material model parameters are selected mainly referring to the previous studies on the dams consisting of similar materials and then back analyses are done to find the best fit. Calculated stresses, displacements and pore water pressures are compared with the observed values for both end of construction and reservoir filling conditions.

Keywords: rockfill dams, displacement, finite element analysis, hardening model, seepage analysis

ÖZ

ÖN YÜZÜ ASFALT KAPLI MURATLI KAYA DOLGU BARAJININ DEFORMASYON DAVRANIŞI ANALİZİ

ÜNSEVER, Yeşim Sema

Yüksek Lisans, İnşaat Mühendisliği Bölümü

Tez Yöneticisi : Prof. Dr. M. Yener ÖZKAN

Ortak Tez Yöneticisi : İnş. Yük. Müh. Gülru S. YILDIZ

Temmuz 2007, 96 sayfa

Bu çalışmada Türkiye'nin ilk ön yüzü asfalt kaplı kaya dolgu barajı olan Muratlı barajının inşa aşamasında ve dolum sırasında oturma davranışı ve temeldeki sızma durumu incelenmiştir. Toplam gerilmelerin, yer değiştirmelerin ve toplam boşluk suyu basınçlarının belirlenmesi amacıyla iki boyutlu düzlem şekil değiştirme prensibi kullanılarak, sonlu elemanlar metodu analizleri gerçekleştirilmiştir. Kaya dolgu malzemesinin doğrusal ve elastik olmayan, gerilme bağımlı davranışını temsil etmek için sertleşen zemin modeli kullanılmıştır. Malzeme model parametreleri, önceki çalışmalar temelinde seçilmiştir ve daha sonra geri analiz yapılarak en uygun parametreler belirlenmiştir. İnşaat sonrasına ve rezervuar dolum aşamasına ait hesaplanan gerilmeler, oturmalar ve boşluk suyu basınçları, ölçülen değerler ile karşılaştırılmıştır.

Anahtar Kelimeler: kaya dolgu baraj, deplasman, sonlu elemanlar metodu, sertleşen zemin modeli, sızma analizi

To My Family

ACKNOWLEDGMENTS

I would like to express my sincere gratitude to my supervisor Prof. Dr. M. Yener ÖZKAN and co-supervisor Gülru S. YILDIZ, M.Sc. for their support, guidance, encouragement and friendly cooperation that they have provided me throughout the study.

I would also like to thank R. Savaş ÖZKUZUKIRAN, M.Sc. for his helpful guidance during the study.

I would like to give my sincere thanks to Ümit for his valuable support, understanding and friendship.

Finally, I would like to offer my special thanks to my parents and my sister for their encouragement, unyielding patience and understanding throughout the study.

TABLE OF CONTENTS

ABSTRACT	iv
ÖZ.....	v
DEDICATION	vi
ACKNOWLEDGMENTS	vii
TABLE OF CONTENTS	viii
LIST OF TABLES	xi
LIST OF FIGURES.....	xiii
CHAPTER	
1. INTRODUCTION	1
2. GENERAL CHARACTERISTICS OF IMPERVIOUS FACE ROCKFILL DAMS	3
2.1 Progress in IFRD	3
2.2 Reasons of the Preference of the IFRD rather than Earth Core Rockfill Dams (ECRD).....	4
2.3 Design of IFRD	5
2.3.1 Specifications for the Design Features of IFRD	5
2.3.2 Zoning of Rockfill Dams with Impervious Face	6
2.3.3 Placement and Compaction of Rockfill	7
2.4 Rockfill Properties	8
2.4.1 Shear Strength of Rockfill Materials	8
2.4.2 Compressibility of Rockfill Materials	10
2.5 Effect of Rock Quality for Compacted Rockfills	11
2.6 Unconfined Compressive Strength of Rock	12
3. NONLINEAR MATERIAL MODELS	13
3.1 Hyperbolic Model	13

3.2 Hardening Model.....	16
4. A REVIEW OF LITERATURE ON THE BEHAVIOR OF ROCKFILL DAMS	18
4.1 Characteristics of Deformation.....	18
4.1.1 General	18
4.1.2 Effect of Reservoir Filling on Rockfill Dams Deformation	20
4.1.3 Assessment of Rockfill Modulus	21
4.1.4 Observed Settlement Behavior of IFRD	23
4.2 Deformation Analyses for Rockfill Dams	26
4.2.1 Application of Finite Element Method on Rockfill Dams	26
4.2.2 Comparison of Two-dimensional and Three-dimensional Finite Element Analysis Results.....	31
4.2.3 Comparison of Measured and Calculated Settlements of IFRD	33
4.3 Seepage for Rockfill Dams	37
4.3.1 Seepage Theory.....	37
4.3.2 Seepage through Rockfill Dams	38
4.3.3 Finite Element Model for Steady-State Seepage	40
5. DEFORMATION AND SEEPAGE ANALYSES OF MURATLI DAM	42
5.1 General Information about Muratlı Dam	42
5.2 Instrumentation in Muratlı Dam	44
5.2.1 Inclinator	52
5.2.2 Fill-extensometer	52
5.2.3 Earthcell	54
5.2.4 Piezometer.....	54
5.3 Stability Analyses of Muratlı Dam	56
5.3.1 Material Model and Parameters	56
5.3.2 Specification for the Analyses	59
5.3.3 Preliminary Analyses	61
5.3.4 End of Construction Analyses	62
5.3.4.1 <i>Vertical Deformations</i>	63

5.3.4.2 <i>Horizontal Deformations</i>	66
5.3.4.3 <i>Total Stresses</i>	68
5.3.5 Reservoir Impoundment Analyses	70
5.3.4.1 <i>Vertical Deformations</i>	71
5.3.4.2 <i>Horizontal Deformations</i>	73
5.3.4.3 <i>Total Stresses</i>	75
5.3.6 Displacement and Stress Contours.....	77
5.4 Pore Pressure in Muratlı Dam	83
6. CONCLUSION	91
REFERENCES	94

LIST OF TABLES

TABLES

Table 2.1 Rock classification according to UCS (Hunter and Fell, 2003).....	12
Table 4.1 E_{rc} and E_{rf} values for selected dams (Fitzpatrick et. al., 1985)	23
Table 4.2 Comparison of plane-strain analysis and three-dimensional analysis (Lefebvre et. al., 1973).....	32
Table 4.3 Stress reduction factors (Hunter and Fell, 2003)	33
Table 4.4 Comparison of calculated and observed settlements for end of construction and reservoir full condition (Özkuzukıran et. al., 2006)	36
Table 4.5 Relative values of soil permeabilities (Singh and Varshney, 1995)	37
Table 5.1 Materials used in the construction of Muratlı Dam	46
Table 5.2 Recorded vertical fill-extensometer values for section A1 (0+200 Km) and A2 (0+300Km)	57
Table 5.3 Hyperbolic stress strain parameters for rockfill material (Khalid et. al., 1990).	58
Table 5.4 Range of stress strain parameters for the model	62
Table 5.5 Stress strain parameters for cross sections A1 and A2	62
Table 5.6 Comparison of calculated and observed vertical deformation values for cross section A1.....	64
Table 5.7 Comparison of calculated and observed vertical deformation values for cross section A2.....	64
Table 5.8 Comparison of calculated and observed horizontal deformation values for cross section A1.....	66
Table 5.9 Comparison of total stresses for cross section A1	69
Table 5.10 Comparison of calculated and observed vertical fill-extensometer values for RI.....	71

Table 5.11 Comparison of calculated and observed horizontal fill-extensometer values for RI.....	74
Table 5.12 Comparison of calculated and observed total stresses for RI	76
Table 5.13 Coefficient of permeability values for Muratlı Dam	84
Table 5.14 Comparison of calculated and observed total heads	89

LIST OF FIGURES

FIGURES

Figure 2.1 Typical zoning of IFRD (Cooke and Sherard, 1987)	7
Figure 2.2 The relation between the normal pressure and friction angle (Leps, 1970)	9
Figure 3.1 Hyperbolic stress-strain curve (Duncan and Chang, 1970)	14
Figure 3.2 Transformed hyperbolic stress-strain curve (Duncan and Chang, 1970)	14
Figure 3.3 Hyperbolic stress-strain curve for hardening model (Schanz et. al., 1999).....	17
Figure 4.1 Reservoir filling effect on a rockfill dam (Nobari and Duncan, 1972).....	20
Figure 4.2 Behavior of El Infiernillo Dam during reservoir filling (Nobari and Duncan, 1972).....	21
Figure 4.3 Assessment of rockfill modulus (Fitzpatrick et. al., 1985).....	22
Figure 4.4 Sections of Shirero Dam (Bodtman and Wyatt, 1985).....	24
Figure 4.5 End of construction settlement of Shirero Dam (Bodtman and Wyatt, 1985).....	24
Figure 4.6 Piezometric levels in fault zone (Bodtman and Wyatt, 1985).....	25
Figure 4.7 Weir flow and effect of silty sand treatment (Bodtman and Wyatt, 1985).....	26
Figure 4.8 Stress distribution of the dam both for single lift and 10-lift increment (Clough et. al., 1967)	27
Figure 4.9 Displacement contours of the dam both for single lift and 10-lift increments (Clough et. al., 1967).....	28
Figure 4.10 Cross section of the dam with material properties (Clough et. al., 1967)	28

Figure 4.11 Variation of horizontal and vertical displacements (Clough et. al, 1967)	29
Figure 4.12 Cross section of Touloustouc Dam (Szostak-Chrzanowski and Massiera, 2006).....	30
Figure 4.13 Calculated horizontal displacements (in meters) of the CFRD on a) rock and b) moraine (Szostak-Chrzanowski and Massiera, 2006).....	30
Figure 4.14 Vertical displacement contours (Lefebvre et. al., 1973).....	31
Figure 4.15 Finite element mesh of Pappadai Dam (Lollino et. al., 2005).....	34
Figure 4.16 Comparison of predicted and measured settlements of Pappadai Dam (Lollino et. al., 2005)	35
Figure 4.17 Finite element mesh of Kürtün Dam (Özkuzukıran et. al., 2006)	36
Figure 4.18 Cross section of Polverina Dam with material zones (Pagano et. al., 2006)	39
Figure 4.19 Piezometer measurements of Polverina Dam (Pagano et. al., 2006).....	40
Figure 4.20 Steady-state seepage flow net for case 1 (Kalkani and Michali, 1984)	41
Figure 4.21 Steady-state seepage flow net for case 2 (Kalkani and Michali, 1984)	41
Figure 5.1 View of Muratlı Dam	43
Figure 5.2 Typical cross section and zoning of Muratlı Dam (dimensions are in meters).....	45
Figure 5.3 Locations of fill-extensometers at section A1 (dimensions are in meters).....	47
Figure 5.4 Locations of fill-extensometers at section A2 (dimensions are in meters).....	48
Figure 5.5 Locations of piezometers, inclinometers and earthcells at section A1 (dimensions are in meters)	49
Figure 5.6 Locations of piezometers, inclinometers and earthcells at section A2 (dimensions are in meters)	50
Figure 5.7 Longitudinal section of Muratlı Dam with the instrument locations.....	51

Figure 5.8 Inclinometer	52
Figure 5.9 Fill-extensometer	53
Figure 5.10 Schematic model of a fill-extensometer	53
Figure 5.11 Earthcell.....	54
Figure 5.12 Piezometer models.....	55
Figure 5.13 Schematic model of a piezometer.....	55
Figure 5.14 Finite element mesh used in the analyses	60
Figure 5.15 Calculated vertical deformations at IC1 and IC2 for section A1.....	65
Figure 5.16 Calculated vertical deformations at IC1 and IC2 for section A2.....	65
Figure 5.17 Calculated horizontal deformations at IC1 and IC2 for section A1	67
Figure 5.18 Observed and calculated displacements for EOC condition.....	67
Figure 5.19 Observed and calculated total stresses for EOC condition.....	69
Figure 5.20 Reservoir impoundment condition for section A1	72
Figure 5.21 Calculated vertical deformations for reservoir impoundment.....	73
Figure 5.22 Calculated horizontal deformations for reservoir impoundment.....	74
Figure 5.23 Observed and calculated displacements for RI condition.....	75
Figure 5.24 Observed and calculated total stresses for RI condition.....	76
Figure 5.25 Horizontal displacements for EOC (in mm).....	78
Figure 5.26 Vertical displacements for EOC (in mm)	78
Figure 5.27 Horizontal stresses for EOC (in kPa)	79
Figure 5.28 Vertical stresses for EOC (in kPa).....	79
Figure 5.29 Shear stresses for EOC (in kPa).....	79
Figure 5.30 Horizontal displacements for RI (in mm).....	81
Figure 5.31 Vertical displacements for RI (in mm)	81

Figure 5.32 Horizontal stresses for RI (in kPa).....	82
Figure 5.33 Vertical stresses for RI (in kPa).....	82
Figure 5.34 Shear stresses for RI (in kPa)	82
Figure 5.35 Total head measurements for Muratlı Dam	83
Figure 5.36 Finite element mesh used in the seepage analyses	85
Figure 5.37 Velocity vectors for EOC (magnified 2.5e+5)	87
Figure 5.38 Pore pressure distribution for EOC.....	87
Figure 5.39 Total head distribution for EOC	87
Figure 5.40 Velocity vectors for RI (magnified 2.5e+5)	88
Figure 5.41 Pore pressure distribution for RI.....	88
Figure 5.42 Total head distribution for RI	88
Figure 5.43 Total head versus distance graph for RI	89
Figure 5.44 Observed and calculated total heads for EOC and RI conditions.....	90

CHAPTER 1

INTRODUCTION

Rockfill dams with impervious face have been preferred since late 1960's due to significant reduction in leakage rate and post-construction deformation (Hunter and Fell, 2003). Construction of an impervious faced rockfill dam (IFRD) has many advantages such as use of local materials, cost-effectiveness, extensive adaptability, simplicity in construction and short construction period.

Although impervious faced rockfill dams have become popular in recent years, the design of these structures is largely based on past experience rather than theory. The most common problem encountered at impervious faced rockfill dam is the cracking of the face membrane, which results in severe leakage.

Finite element method (F.E.M.) is used to assess the stresses and deformations in earth and rockfill dams for both construction and reservoir filling conditions. In the past, linear elastic theory was applied to analyze soil behavior although it does not approximate the real soil behavior well due to past insufficiency in computer technology. However soil behavior is modeled by nonlinear, inelastic models nowadays. It is possible to use numerical analysis techniques such as finite element method developed by Clough (1967) by the help of high speed computers. Therefore, the soil model is similar to the real soil behavior.

Predicted and observed values are compared to understand the validity of the design. In modeling of a dam, the selection of the model and the geotechnical parameters are important. However, the assessment of the properties of rockfill is difficult due to large particle dimensions used in rockfill dams and capacity of test equipment.

Therefore, parameters have to be defined by previous dam data or back analyses of field response.

In this study the behavior of Muratlı Dam, the first asphalt faced rockfill dam in Turkey is examined. Plain strain analysis is carried out since two-dimensional analysis can be applicable for dams which have large length/height ratio. The analyses are made by using Plaxis v7.2 finite element program to compute stresses and deformations both for construction and full reservoir loading conditions. In addition, Seep-W seepage program is used to evaluate the pore pressure distribution in the foundation and in the body of the dam for both end of construction and reservoir filling cases.

Rockfill behavior is nonlinear, inelastic and stress dependent. In order to capture these features, hardening model is selected to model the dam. The model parameters are estimated by making use of the results obtained by the previous studies as well as the back analyses made by utilizing the measured data.

In Chapter 2, general information on impervious faced rockfill dams are given. In Chapter 3, the nonlinear material model used in the analysis is summarized. Chapter 4 reviews behavior of rockfill dams and finite element method applications. The analyses results and the comparison with the observed values are given in Chapter 5. The conclusions derived are represented in Chapter 6.

CHAPTER 2

GENERAL CHARACTERISTICS OF IMPERVIOUS FACED ROCKFILL DAMS

Since rockfill dam is a type of embankment dam, impermeability is provided either by an impervious material or by an impervious core. The location of the impervious membrane and the material type of the membrane is selected according to the site conditions and dam properties.

2.1 Progress in IFRD:

Cooke (1984) classified the progression of rockfill dams in three distinct periods:

- 1) Early Period (1850-1940): The date of construction of the first modern dam goes back to California gold rush times. These dams had timber faces and very steep slopes. In the dam body, dumped rockfills were used and the height of the dams were maximum 25 m. These dams had good performance but the leakage was a serious problem when the dams became higher.
- 2) Transition Period (1940-1965): Since dumped rockfill dams with impervious membrane had serious problems and certain limitations, a transition was made to compacted rockfill with both earth core and impervious-faced dams. The unavailability of suitable rockfill materials which require high unconfined compressive strength for higher dams was the major consideration in this period.
- 3) Modern Period (1965-): In this period, compaction has become universal in rockfill dams although the use of dumped rockfills is continued at side zones and in cofferdams. Compacted rockfill has many advantages, such as the

possible use of relatively weak rocks and construction of higher dams. This transition from dumped rockfill to compacted rockfill increased the use of relatively low strength rock types, relatively thin face slabs and also decreased the amount of reinforcement in the face slab (Cooke, 1984).

2.2 Reasons of the Preference of the IFRD rather than Earth Core Rockfill Dams (ECRD):

As mentioned in Chapter 1, IFRD are preferred in recent years. The reasons for preferring IFRD rather than ECRD are illustrated below (Cooke and Sherard, 1987):

- Although the required site conditions (good rock foundation) are similar for both dams, IFRD is least cost alternative.
- IFRD is preferable when the earth core material is not available.
- IFRD has significant advantage in the sites with rainy climatic conditions.
- The steeper slopes can be applied to IFRD.
- IFRD can be built more rapidly due to independency to weather conditions and smaller volume of the body.
- Leakage in IFRD is not a safety problem, the matter is economical. However for ECRD, leakage can endanger safety and should be monitored during the whole life of the structure.
- For IFRD, the treatment of the foundation is usually under the toe slab, whereas for ECRD the treatment is generally under the earth core, which corresponds to a larger area.
- Any unexpected flood during construction does not affect the IFRD much. Because the friction angle forces due to rock to rock contacts are greater than the hydraulic forces due to water flow.
- IFRD are proved to be safe under dynamic loads.

2.3 Design of IFRD:

2.3.1 Specifications for the Design Features of IFRD

Toe Slab: Toe Slab is placed on hard rock which is groutable. The main purpose is to eliminate possible erosion of the foundation. The width of toe slab is approximately $1/20$ - $1/25$ of the water depth, and minimum width is 3 m. The thickness of toe is usually equal to the face slab thickness, which is about 0.3-0.4 m. The main point during the construction of the toe slab is the bond between the slab and rock. It may be obtained by cleaning and wetting the rock surface (Cooke and Sherard, 1987).

Face Slab: The main concern in an IFRD is the settlement of the dam body. The face should be designed as not to be cracked under the reservoir water load. The most common material for facing is concrete, followed by asphaltic concrete. The material selection of the slab can be done according to the height of the dam. Asphaltic-concrete, which is the second most common material type for the facing, can be used up to moderate height dams where concrete is selected as a face material for higher dams (Cooke and Sherard, 1987).

Important points that should be considered for the design of face slab of IFRD (Fitzpatrick et. al., 1985):

- The dam body should be completed before the construction of the face to avoid large cracks at the face slab.
- The thickness of the face slab does not have significant effect on the strains which occurs in the face slab. Thickness of the slab should be decided by considering impermeability and economical life.
- Strains occurred in the face slab can be reduced by effective placement of rockfill such as wetting during compaction.

- Joints should be used between slab and rockfill to limit the opening due to water load effect (joints are only necessary for concrete membranes).
- Plinth which provides watertight connection should be used between the face slab and dam foundation.

Foundation: Measurements showed that the influence of the reservoir load on downstream part of the dam is very small. Generally soil on the hard rock is excavated before the construction of high dams, whereas soil is left in place for low to moderate high dams. This is also the case for alluvium deposits. Problems encountered with such foundations are liquefaction and seepage. Settlement is not a problem since alluvium has high modulus of compressibility. As an example, alluvial gravels were not excavated in the Lower Pieman Dam foundation. The deformation modulus of the alluvium under embankment loading was assessed to be approximately 200 MPa. This value is higher than most of the compacted rockfill materials' moduli (Fitzpatrick et. al., 1985).

2.3.2 Zoning of Rockfill Dams with Impervious Face

Typical zoning of IFRD is shown in Figure 2.1. Zone 1 consists of impervious soil, which covers the joints and slab. Also this zone limits the leakage in the face slab. There are dams without Zone 1. Zone 2 is used to provide uniform support for the face of the dam. It is also useful to provide semi-impervious layer which prevents large leakages when a crack occurs on the slab. Zone 3 consists of three sub-zones. Zone 3A is a transition zone between Zone 2 and Zone 3B. The main purpose of this zone is to prevent material transition from Zone 2 to main rockfill. Zone 3B is the main part of the dam body. The most important point to be considered during construction of this zone is to minimize the compressibility for reduction of slab settlement due to water load. Zone 3C has little effect on dam performance since it takes negligible water load. In this zone, the rockfill is placed in thicker layers than Zone 3B (Cooke and Sherard, 1987).

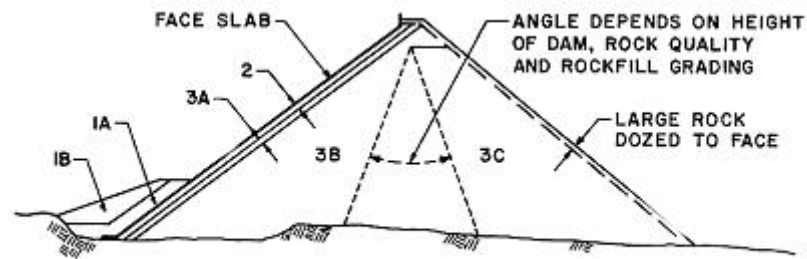


Figure 2.1: Typical zoning of IFRD (Cooke and Sherard, 1987)

2.3.3 Placement and Compaction of Rockfill

There are two methods for the placement of rockfill; dumped and compacted (Hunter and Fell, 2003):

- Dumped rockfill: The placement of rockfill is done without compaction in lifts ranging from several to ten meters thickness, with or without sluicing.
- Compacted rockfill: The placement of rockfill is done by compacting with four to six passes of a smooth drum vibrating roller (SDVR) in layers up to 2 m thickness (generally 0.9 to 2 m thick) with added water. The deadweight of the vibrating roller is a minimum of 10 t. Compacted rockfill can be classified in three groups:
 - Well-compacted: The thickness of the layer is generally less than 1 m depending on the intact strength of the rock. The placement is usually done with a 10 t deadweight SDVR, compaction is carried out usually with a minimum four passes, with the addition of water.
 - Reasonable compacted: The thickness of the layer is generally between 1.5 to 2 m depending on the intact strength of the rock. The placement is usually done with a 10 t deadweight SDVR, compaction is carried out usually with four passes, without the addition of water.
 - Reasonable to well compacted: The thickness of the layer is generally between 1.2 to 1.6 m depending on the intact strength of the rock. The

placement is usually done with a 10 t deadweight SDVR, compaction is carried out usually with four to six passes, with the addition of water.

2.4 Rockfill Properties:

Shear strength and compressibility are the most important parameters when rockfill properties are considered.

2.4.1 Shear Strength of Rockfill Materials

Large scale triaxial testing equipment is required to assess the real behavior of rock material. This apparatus is used to obtain stress-strain properties of rockfill under high lateral pressures. However, performing a test on rockfill material with real size is generally impossible due to the heavy cost of this equipment. In order to test such materials, the size of the sample can be reduced, but the grading should be similar with the original one. Testing the larger size of the material is an important matter to define the material properties because angle of friction of the material depends on the size of the material. As the angle of friction decreases, the size and stresses of the system increases (Fumagalli, 1969).

A study was shown that the specific rockfill material has different friction angles at different confining pressures such as in the case of El Infiernillo Dam. Here, rock material's friction angle is 50° at 5.7 psi and 34° at 355 psi (Leps, 1970, after Marshal, 1967). The dependency of friction angle on normal pressure is illustrated in Figure 2.2.

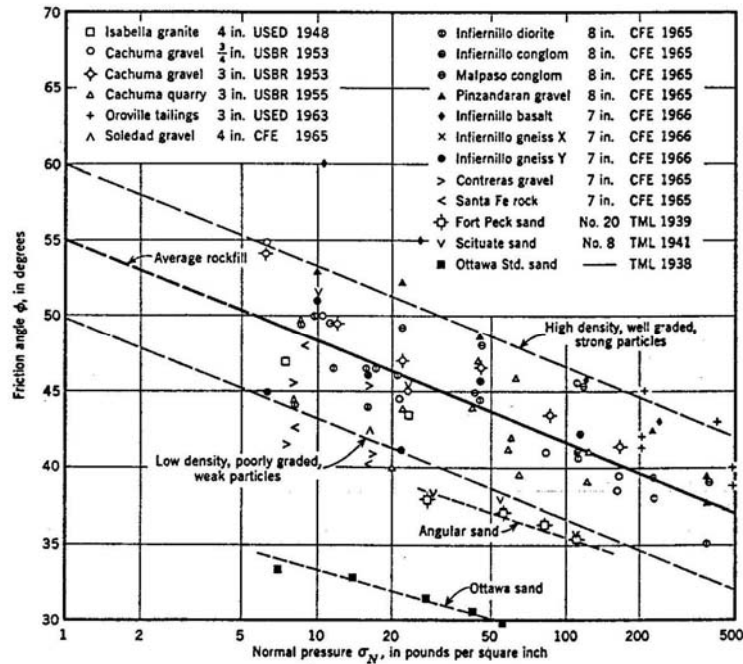


Figure 2.2: The relation between the normal pressure and friction angle (Leps, 1970)

Other properties which affect the shear strength of rockfill material are (Leps, 1970):

- Relative Density: An increment in the relative density causes an increase in friction angle at a constant normal pressure.
- Gradation: An improvement in the gradation of rockfill causes an increase in friction angle at a constant normal pressure.
- Particle Shape: An increment in the amount of angular particles causes an increase in the strength of material.
- Degree of Saturation: An increment in the degree of saturation of the particles causes a decrease in the strength of material.
- Particle Size: There is some divergence about the effect of the particle size. A decrement in particle size by scalping technique (remove all material above a certain size) causes an increase in friction angle. However, if particle

size is decreased by parallel gradation technique, friction angle will also decrease (Singh and Varshney, 1995).

2.4.2 Compressibility of Rockfill Materials

In rockfill dams, another important parameter to be considered is the compressibility of rockfill material. When impervious faced rockfill dam is considered, this concept becomes important since large movements in the dam might cause cracking at the impervious face. The compressibility of the rockfill can be assessed by considering the following points (Saboya and Byrne, 1993):

- Uniformity coefficient (C_u): Defined as the ratio of D_{60} to D_{10} , where D_{60} and D_{10} are the particle sizes corresponding to 60% and 10% finer by weight. Uniform rockfills are more compressible than well-graded rockfills, because of having less contact area, resulting in high contact forces.
- Grain shape: Angular grains are more compressible than rounded grains. Because they are in a more breakable manner.
- Relative Density (D_r): Denser rockfill is less compressible, because of having more contacts, resulting small contact forces. Also rearrangement is less for dense rockfill which also reduces compressibility.
- Grain size: Large grains are more compressible than small grains, due to the higher contact forces and tendency to breakage. Also, large grains have lower shear strength than small grains for the same uniformity coefficient. It should be noted that the results obtained from laboratory tests should be corrected for the grain size in the field.
- Mineralogy: It was indicated that mineralogy has an important effect on the breakage index of rockfill mass, which also controls compressibility (Saboya and Byrne, 1993, after Marshal, 1973).

2.5 Effect of Rock Quality for Compacted Rockfills:

There is no limitation for the rock quality for compacted rockfills. Any type of rock including soft rock which has ability to support construction trucks and a 10 ton vibratory roller is acceptable. Rockfill modulus is a useful parameter to decide on the suitability of rockfill in construction of a dam. In general, granites, diorites, gneisses, basalts, dense sandstones and limestones, dolomitic quartzites and massive schists are used, but also in several medium height dams, weak rocks such as siltstones, schists and argillites have been used (Singh and Varshney, 1995). All hard and weak rocks have some advantages and disadvantages. The following comparison can be done between the weak and hard rocks (Xing et. al., 2006):

- During the compaction procedure, weak rocks can easily be crushed into smaller particle size than hard rocks.
- Higher densities can be reached for weak rocks than hard rocks due to the breakdown of the particles during compaction.
- Compared to weak rocks, hard rocks do not deform easily. As a result, deformations in hard rock dams are smaller than the deformations in weak rock dams.
- Due to the smaller particle size of the weak rocks after compaction, they have lower permeability than hard rocks.
- Sluicing contributes to the breakdown of the weak rocks and increases the smaller particle size, resulting in strength reduction, which is not the case for hard rocks. Therefore, the water content used during compaction should be controlled during the construction of weak rocks.
- Weak rocks have well graded particle-size distribution compared to hard rocks.

2.6 Unconfined Compressive Strength of Rock:

Australian Standard AS 1726-1993 is used for classification of the unconfined compressive strength (UCS) of intact rock used in rockfill. Classification of rock according to UCS is given in Table 2.1. Generally, medium to high strength rock is used in compacted rockfill. Rocks with higher strength do not have any technical advantage (Hunter and Fell, 2003).

Table 2.1: Rock classification according to UCS (Hunter and Fell, 2003)

Rock Classification	Unconfined Compressive Strength Value (UCS) (MPa)
Extremely High Strength	$UCS > 240$
Very High Strength	$70 < UCS < 240$
High Strength	$20 < UCS < 70$
Medium Strength	$6 < UCS < 20$

CHAPTER 3

NONLINEAR MATERIAL MODELS

As it is mentioned in previous sections, nonlinear, inelastic and stress-dependent models are more realistic in modeling the dams. In this study, hardening soil model is selected as a nonlinear model. Hardening model is based on Duncan and Chang's hyperbolic model. In the following sections, main features of hyperbolic and hardening models are summarized.

3.1 Hyperbolic Model:

The nonlinear material properties of rockfill are based on hyperbolic stress-strain function which was developed by Kondner (1963) and extended by Duncan and Chang (1970) and Kulhawy and Duncan (1972). The used failure criterion is Mohr-Coulomb.

The hyperbolic stress-strain curve is shown in Figure 3.1, where σ_1 and σ_3 are the major and minor principal stresses, ϵ is the axial strain, E_i is the initial tangent modulus and a and b are the experimentally defined constants. If Figure 3.1 is plotted as shown in Figure 3.2, a and b can be defined more easily (Duncan and Chang, 1970).

Asymptotic value of the hyperbole may be related to the compressive strength by means of a factor R_f by using the following equation:

$$(\sigma_1 - \sigma_3)_f = R_f \cdot (\sigma_1 - \sigma_3)_{ult} \quad \text{(Equation 3.1)}$$

where,

$(\sigma_1 - \sigma_3)_f$: compressive strength or stress difference at failure

$(\sigma_1 - \sigma_3)_{ult}$: asymptotic value of stress difference

R_f : failure ratio (between 0.75 and 1.00 and independent of confining pressure)

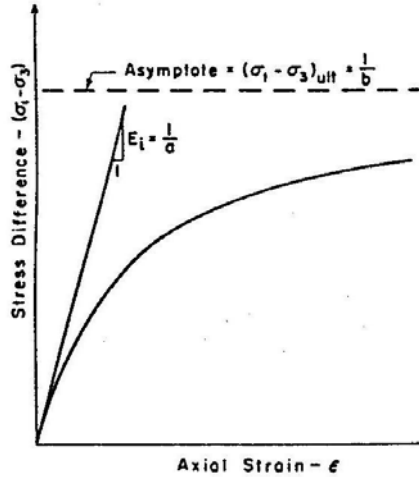


Figure 3.1: Hyperbolic stress-strain curve (Duncan and Chang, 1970)

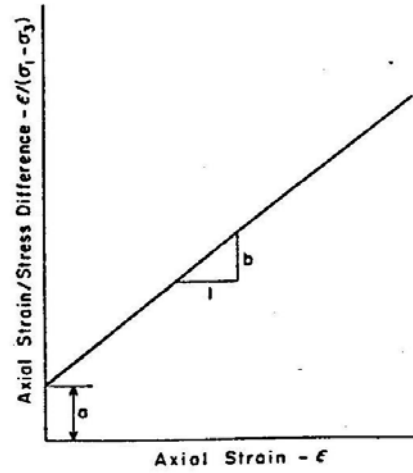


Figure 3.2: Transformed hyperbolic stress-strain curve (Duncan and Chang, 1970)

Initial tangent modulus, E_i is defined by experimental studies of Janbu (1963) as

$$E_i = K \cdot p_a \left(\frac{\sigma_3}{p_a} \right)^n \quad \text{(Equation 3.2)}$$

where,

p_a : atmospheric pressure

σ_3 : minor principal stress

K : modulus number

n : hyperbolic exponent

The expression for tangent modulus of elasticity which is based on Duncan and Chang stress-strain model that was first proposed by Kondner (1963) is:

$$E_t = (1 - R_f \cdot m)^2 \cdot E_i \quad (\text{Equation 3.3})$$

where,

E_t : tangent modulus of elasticity at a particular stress level

R_f : failure ratio

m : mobilization factor, defined as $(\sigma_1 - \sigma_3)/(\sigma_1 - \sigma_3)_f$

E_i : initial modulus of elasticity for a particular confining pressure

When Mohr-Coulomb failure criterion is used to express tangent modulus of elasticity, the formula becomes,

$$E_t = \left[1 - \frac{R_f (1 - \sin \phi) (\sigma_1 - \sigma_3)}{2c \cdot \cos \phi + 2\sigma_3 \sin \phi} \right]^2 \cdot E_i \quad (\text{Equation 3.4})$$

where,

c : cohesion of the soil

ϕ : angle of internal friction

σ_1, σ_3 : major and minor principal stresses

Kulhawy and Duncan (1972) developed an expression for tangent Poisson's ratio ν_t to represent the volume changes during the triaxial compression test. The formula of the expression is:

$$\nu_t = \frac{G - F \cdot \log\left(\frac{\sigma_3}{p_a}\right)}{\left\{ 1 - \frac{d \cdot (\sigma_1 - \sigma_3)}{K \cdot p_a \left(\frac{\sigma_3}{p_a}\right)^n \left[1 - \frac{R_f \cdot (1 - \sin \phi) \cdot (\sigma_1 - \sigma_3)}{2 \cdot c \cdot \cos \phi + 2 \cdot \sigma_3 \sin \phi} \right]} \right\}^2} \quad (\text{Equation 3.5})$$

where,

G, F, d : Poisson's ratio parameters

3.2 Hardening Model:

Although hyperbolic model captures soil behavior well and application of the model is much appreciated, the model has a major weak point due to not separating the loading and unloading conditions. Hardening model is the improved form of hyperbolic model. This new constitutive model is based on theory of plasticity rather than theory of elasticity. And also it takes soil dilatancy into account (Schanz et. al., 1999).

The hyperbolic relationship between the vertical strain ε_1 , and the deviatoric stress q can be approximated by the following formula using drained triaxial test,

$$\varepsilon_1 = \frac{q_a}{2E_{50}} \cdot \frac{(\sigma_1 - \sigma_3)}{q_a - (\sigma_1 - \sigma_3)} \quad \text{for } q < q_f \quad (\text{Equation 3.6})$$

where,

q_f : ultimate deviatoric stress,

q_a : asymptotic value of shear strength

E_{50} : confining stress dependent stiffness modulus for primary loading

q_f and q_a are defined as:

$$q_f = \frac{6 \sin \phi_p}{3 - \sin \phi_p} (p + c \cot \phi_p) \quad q_a = \frac{q_f}{R_f} \quad (\text{Equation 3.7})$$

where,

c, ϕ_p : strength parameters

For the primary loading, the parameter E_{50} is used as a tangent modulus, which is dependent on the confining pressure. The equation of the E_{50} is:

$$E_{50} = E_{50}^{ref} \left(\frac{\sigma_3 + c \cot \phi_p}{\sigma^{ref} + c \cot \phi_p} \right)^m \quad (\text{Equation 3.8})$$

where,

σ^{ref} : reference pressure

m: amount of the stress dependency

E_{50}^{ref} : reference stiffness modulus corresponding to the reference stiffness, p^{ref}

This relationship is shown in Figure 3.3. When failure occurs, $q=q_f$; perfectly plastic yielding is observed which causes irreversible plastic strain. R_f should be smaller than 1.0, and can be taken as 0.9 by default setting. The stress dependency parameter m is taken as 1.0 for soft soils and taken as 0.5 for hard soils (Schanz et. al., 1999).

For unloading and reloading conditions, the parameter E_{ur} is used. The equation of the E_{ur} :

$$E_{ur} = E_{ur}^{ref} \left(\frac{\sigma_3 + c \cot \phi_p}{\sigma^{ref} + c \cot \phi_p} \right)^m \quad (\text{Equation 3.9})$$

where,

E_{ur}^{ref} : the reference stiffness modulus for unloading and reloading corresponding to the reference pressure, σ^{ref}

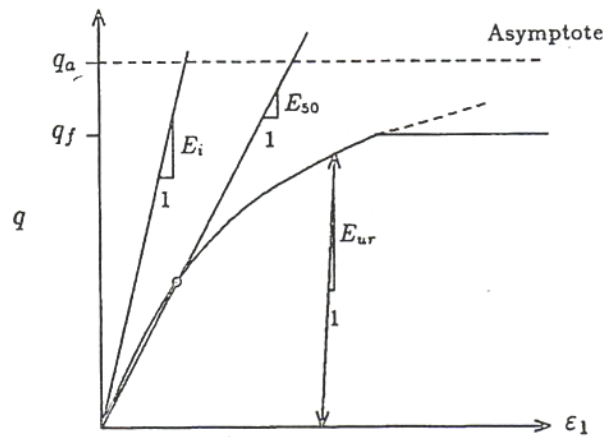


**Figure 3.3: Hyperbolic stress-strain curve for hardening model
(Schanz et. al., 1999)**

CHAPTER 4

A REVIEW OF LITERATURE ON THE BEHAVIOR OF ROCKFILL DAMS

Deformation of a rockfill dam starts with the commencement of the construction which causes an increase of the effective stresses. Further deformations are caused due to the first filling of the reservoir. Upon the reservoir filling the rate of deformation decreases except the fluctuations on the water level. The deformations of a rockfill dam can be considered in terms of vertical and horizontal components. Horizontal deformations can also be considered in two categories namely, in upstream-downstream direction and in cross-valley direction.

Since in IFRD, the impermeability of the dam mainly depends on the impermeability of the slab, any cracks on the slab may cause problems in the dam body. For these type of dams, the most critical deformation is the one on the face slab. This is the reason why, the face slab is constructed after the completion of the dam body to prevent large cracks due to settlement of the body.

4.1 Characteristics of Deformation:

4.1.1 General

Monitoring of deformations of the dam may be helpful to assess the safety of the dam. Failures generally send warning signals such as increased rate of deformation, strain discontinuities, cracking, leakage or pore-pressure build-up.

Rockfill dams which are constructed with sound, hard, well-graded rock and formed in layers of small thicknesses are expected to experience relatively small

deformations. The larger portion of the settlement takes place during construction (Singh and Varshney, 1995).

Settlements of fourteen rockfill dams were studied and it was reported that the range of settlement in ten years, ranged between 0.25% and 1% of the dam height. Also it was noted that this ratio is independent of the height and rockfill characteristics. It only depends on the construction method, for example sluicing during construction is an important factor in reducing the settlements (Dascal 1987, after Sowers et. al., 1965).

Deformation of rockfill dams continues upon completion of the construction with a decreasing rate. The maximum post-construction settlement of a dam was given with the following formula:

$$S = 0,001H^{3/2} \quad \text{(Equation 4.1)}$$

where S is the total settlement of the dam and H is the height of the dam, both in meters. They also concluded that 85 % of the settlement occurs in the first year for impervious faced dams with rapid reservoir impoundment. However, the first year settlement rate decreases for the dams with impervious core and relatively slow reservoir impoundment (Dascal, 1987, after Lawton and Lester, 1964).

Another study was also done on dam behavior and it was suggested that the data of the dams with similar characteristic can be used to predict the behavior of a dam (Dascal, 1987, after Clements, 1984).

In practice, it can be said that total settlement is reached when the annual settlement percentage of the dam is less than 0.02H %. The studies of Dascal (1987) showed that the settlement is completed approximately in 24-30 months after the end of construction.

As mentioned before, horizontal deformations can be grouped in two categories. The first one is the cross-valley horizontal deformation which occurs due to the self-weight of the dam. Cross-valley deformation results in horizontal tension in the membrane near the joints. The second one is upstream-downstream direction horizontal deformation which occurs due to the first filling of reservoir resulting in additional vertical and horizontal deformation (Singh and Varshney, 1995).

4.1.2 Effect of Reservoir Filling on Rockfill Dams Deformation

The researchers found that generally the most serious damages such as large horizontal and vertical movements in a dam occur due to reservoir filling. Such large movements arise because of two main reasons. First one is the water loads on the dam and second one is the softening and weakening of the fill material due to wetting. (The first reason of these movements can be simulated with standard finite element method, whereas the second may not.) The softening and wetting is generally considered in earth dams due to the significant changes in stresses at the wet parts of the dam (Nobari and Duncan, 1972).

The reservoir filling effects are shown in Figure 4.1. First three figures indicate the water load, and the last indicates the softening and weakening.

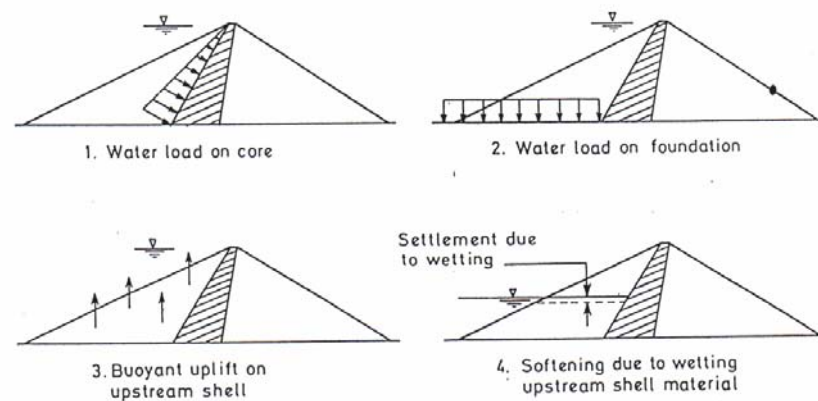


**Figure 4.1: Reservoir filling effect on a rockfill dam
(Nobari and Duncan, 1972)**

Deformations due to reservoir filling in the core of El Infiernillo Dam are shown in Figure 4.2. It can be seen that the first movement of the core occurred due to the softening of the upstream shell material when the reservoir elevation was raised from 80 m to 120 m, where the direction of the deformations was towards upstream. Then, a small downstream movement occurred when the water level reached to 160 m. Finally, when the water level rose to the level of 170 m, a large downstream movement occurred. At the beginning of the reservoir filling, the softening was dominant. But when the second part of the filling is considered, water load was dominant (Nobari and Duncan, 1972).

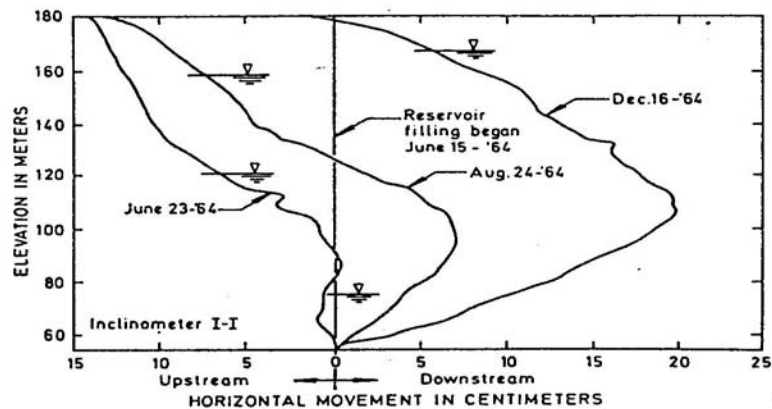


**Figure 4.2: Behavior of El Infiernillo Dam during reservoir filling
(Nobari and Duncan, 1972)**

4.1.3 Assessment of Rockfill Modulus

Fitzpatrick et al. (1985) defined two rockfill moduli to represent the deformation behavior of the rockfill; one is used to define construction behavior, E_{rc} and the other is used to define first filling behavior, E_{rf} of the dam (Fig. 4.3). The equations for E_{rc} and E_{rf} are shown below:

$$E_{rc} = \gamma.H.d_1 / \delta_s \quad (\text{Equation 4.2})$$

$$E_{rf} = \gamma_w.h.d_2 / \delta_n \quad (\text{Equation 4.3})$$

where E_{rc} and E_{rf} are in Mpa, γ (unit weight of the rockfill) in kN/m^3 , δ_s (settlement in millimeters of the thickness d_1 due to the construction of H shown in Figure 4.3) and δ_n (deflection in millimeters of the face slab at depth h from the reservoir surface due to the reservoir filling), where H , h , d_1 and d_2 are in meters. It should be noted that, E_{rf} is only used to estimate the face slab deformations; it is not a “real” modulus number (Hunter and Fell, 2003).

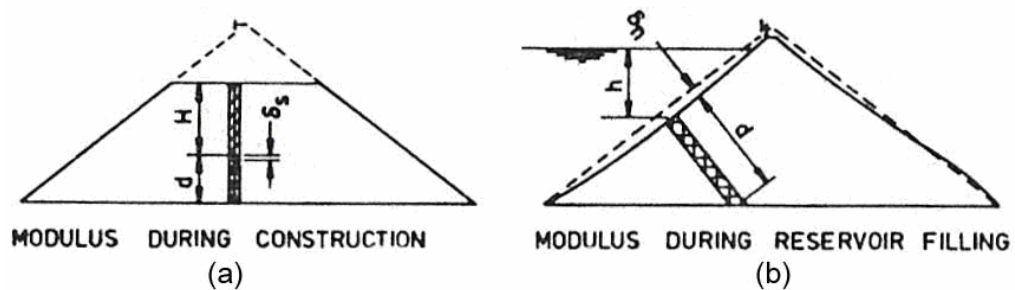


Figure 4.3: Assessment of rockfill modulus (Fitzpatrick et. al., 1985)

E_{rc} and E_{rf} values for some selected dams are given in Table 4.1. It can be seen that the modulus that measured during the construction is not the same as the one measured during reservoir filling. The modulus measured during reservoir filling is generally greater than the modulus measured during construction when the reservoir impoundment is completed in a short period. It is not the case when the reservoir impoundment is completed in a long period (Fitzpatrick et. al., 1985).

Table 4.1: E_{rc} and E_{rf} values for selected dams (Fitzpatrick et. al., 1985)

Name of Dam	Rock Type	Modulus E_{rc} (Mpa)	Modulus E_{rf} (Mpa)
Wilmot	Greywacke-Quartzite	115	160
Cethana	Quartzite	145	310
Paloona	Chert	75	115
Serpentine	Quartzite	115	95
Mackintosh	Greywacke	40	95
Tullabardine	Greywacke	90	170
Murchison	Rhyolite	225	650
Bastyan	Rhyolite	160	300
Lower Pieman	Dolerite	160	-

4.1.4 Observed Settlement Behavior of IFRD

A case study is selected to present the behavior of dam both during construction and reservoir filling. Shirero Dam, a concrete faced rockfill dam, constructed across the Kaduna River in Nigeria is considered. The dam has a maximum height of 125 m and a crest length of 560 m. The grout curtain was constructed under the toe slab, which was extended to a depth equal to at least 2/3 of the reservoir head above the foundation (Bodtman and Wyatt, 1985).

Figure 4.4 shows the profile and maximum section of the dam. The dam contains four zones of rockfill material; Zone 1, Zone 2, Zone 3 and Zone 2A (transition zone). Rockfill material was selected from on-site quarries which were sound granite.

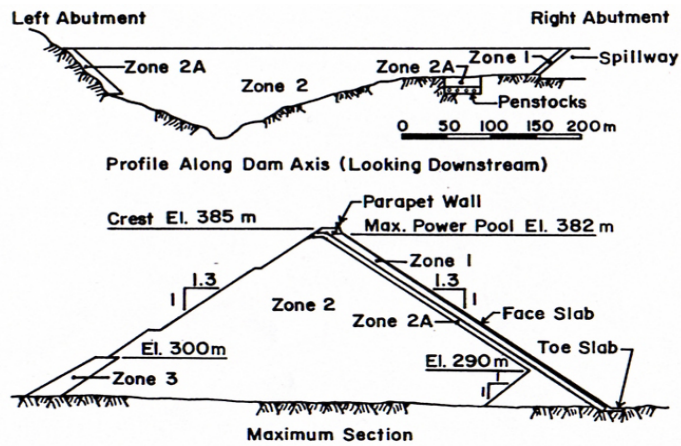


Figure 4.4: Sections of Shiroro Dam (Bodtman and Wyatt, 1985)

Deformation of the face slab due to settlement was minimized by the completing the dam to elevation 381.5 m (crest elevation=385 m) before the placement of the face slab concrete. During construction, the performance of the dam was directed toward measuring settlements and horizontal deformations. End of construction settlements are shown in Figure 4.5. Maximum settlements occurred near the mid-height of the dam. The greatest settlement at the elevation 381.5 m, in March 1983, was 0.84 m at the inclinometer located near the valley center. Additional settlements of 0.10 m occurred due to both creep and the final 3.5 m embankment placed in early 1984 (Bodtman and Wyatt, 1985).

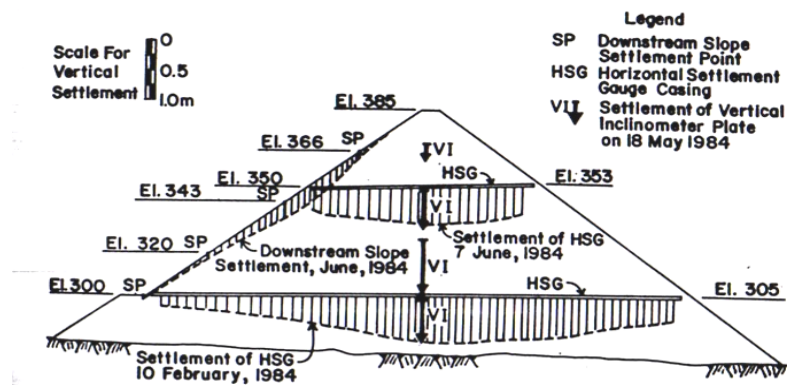


Figure 4.5: End of construction settlement of Shiroro Dam (Bodtman and Wyatt, 1985)

After impounding of the reservoir, all the piezometers installed in the fault zone, upstream and downstream of the grout curtain, indicated a rise in piezometric level. Piezometers located near the downstream toe of the dam showed negligible response to reservoir impounding. Average piezometric levels of upstream and downstream of the grout curtain and at the downstream of the toe with the reservoir at elevation 372 m is shown in Figure 4.6. It is obvious that grout curtain has a significant effect on reducing the piezometric pressures and seepage.

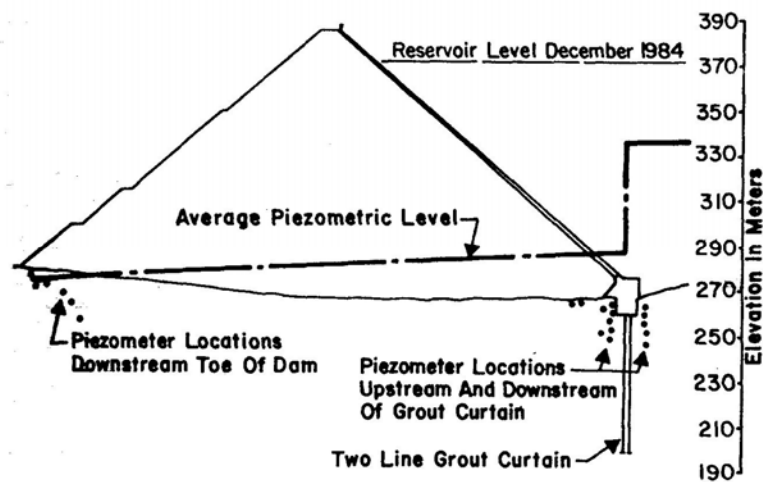
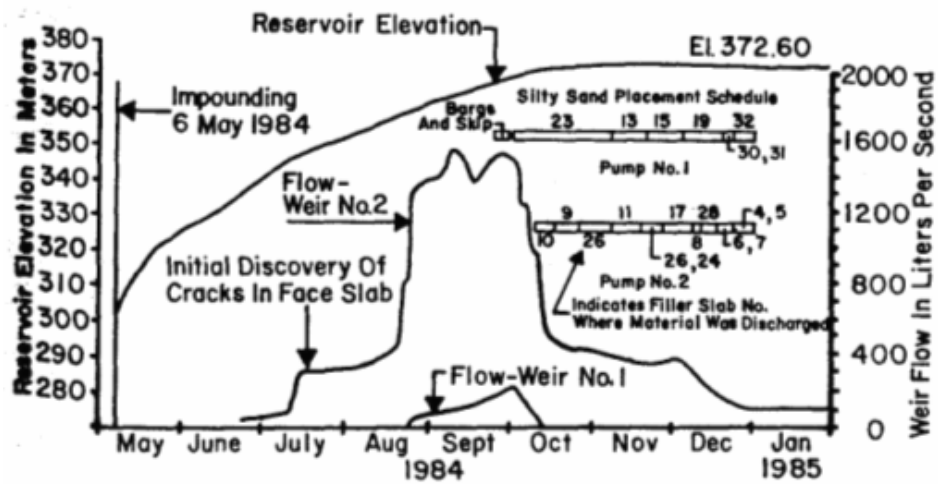


Figure 4.6: Piezometric levels in fault zone (Bodtman and Wyatt, 1985)

The records of flow through the two weirs are shown in Figure 4.7 with the corresponding reservoir level. To investigate the increased flow in Weir No. 2, an underwater inspection of the dam face slab was done. Cracks were observed at the lower corner of the face slab. Leakage from these cracks was reduced by depositing a silty sand filter material at the cracked locations. With the major sources of leakage treated; seepage at Weir Box 1 dried up completely and Weir Box 2 reduced to 100 L/sec by the end of 1984 (Bodtman and Wyatt, 1985).



**Figure 4.7: Weir flow and effect of silty sand treatment
(Bodtman and Wyatt, 1985)**

4.2 Deformation Analyses for Rockfill Dams:

4.2.1 Application of Finite Element Method on Rockfill Dams

Rockfill dams are analyzed to define the stresses and deformations both in the dam and its foundation. During the analyses, the system is generally assumed as a two-dimensional plane-strain problem which is actually three dimensional. Another point that should be taken into account is the embankment which is constructed by incremental processes. In finite element analysis, discrete elements which are connected at their nodal points are used to idealize the actual continuum. Also in two-dimensional analysis, using of triangular plate elements (which is the case in F.E.M. software Plaxis) is convenient for idealization of the actual dam behavior. In finite element plane strain analysis, compatibility and equilibrium conditions should be satisfied. The procedure of the analyses is as follows: first the stiffness of the lowest layer of elements and their dead loads are evaluated, and then stresses and displacements occurred due to the construction of this layer are calculated. The same procedure goes on up to the last stage of construction (Clough et. al., 1967).

The comparison of horizontal and vertical normal stresses and shear stresses for a single lift and 10-lift with linear-elastic analysis are shown in Figure 4.8. It can be observed that, the differences between two analyses are very small which is also the case for horizontal displacements.

However, when the vertical displacements are concerned, the deformation mechanisms are different (Figure 4.9). The largest deformation occurs at the crest for “the single lift analysis”, whereas the results for “10-lift analysis” show that the largest vertical deformation occurs approximately at the mid-height of the dam.

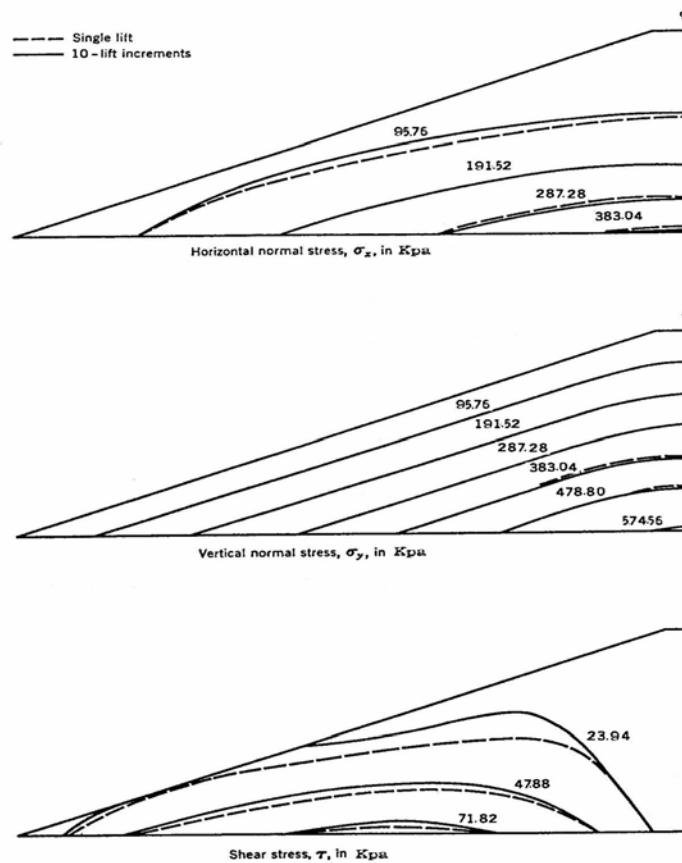


Figure 4.8: Stress distribution of the dam both for single lift and 10-lift increment (Clough et. al., 1967)

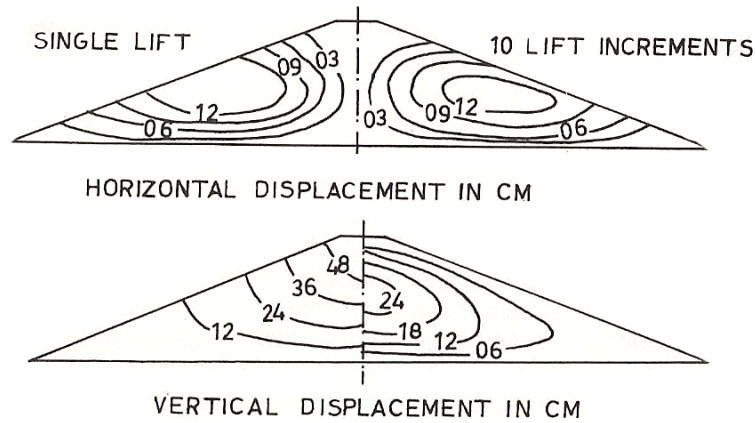


Figure 4.9: Displacement contours of the dam both for single lift and 10-lift increments (Clough et. al., 1967)

Up to this point, the flexibility of the foundation is not included in the analysis. However, in practice the foundation is not perfectly rigid. Therefore, the effect of flexibility of foundation should be examined also. The dam was reexamined by Clough et. al. (1967) with flexible foundation, depth of which is equal to the half of the dam height (Figure 4.10).

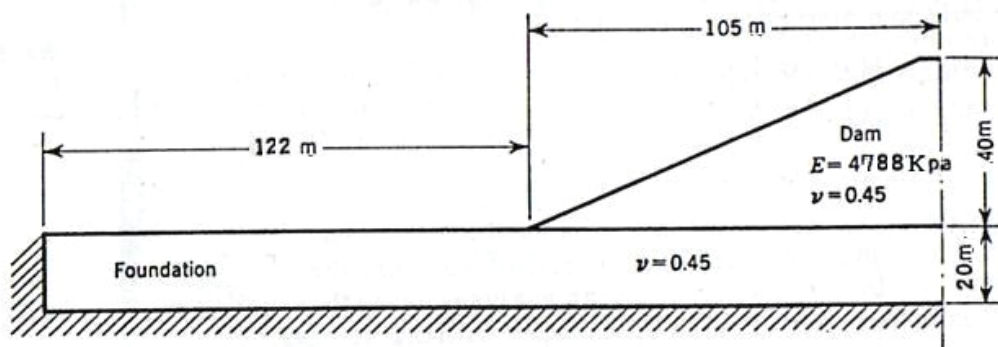
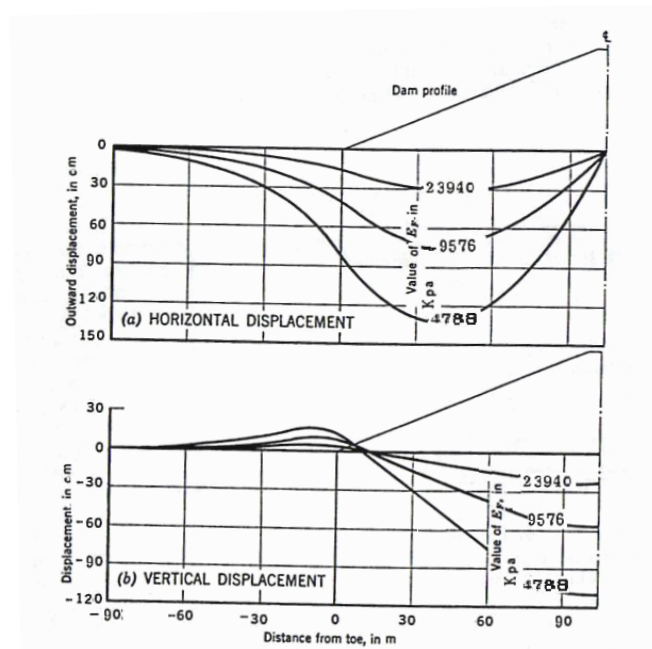


Figure 4.10: Cross section of the dam with material properties (Clough et. al., 1967)

In the analysis, four different elastic moduli (4788, 9576, 23940 kPa and rigid) were defined for the foundation. The effect of modulus of elasticity of foundation on stresses was examined. It was observed that, vertical stresses are not affected by the modulus of elasticity. On the contrary, horizontal stresses and shear stresses are affected significantly.

Generally, stresses and displacements are inversely dependent on each other, such as when stresses are increased, displacements are reduced or vice versa. The effect of modulus of elasticity of foundation on horizontal and vertical displacements is shown in Figure 4.11.

Another study was done by Szostak-Chrzanowski and Massiera (2006) on foundation flexibility of Toulnostouc Dam, located on the Toulnostouc River in Northern Quebec. The height and the crest length of the dam are 75 m and 0.575 km, respectively. The dam was built on bedrock with a slab thickness of 0.3 m. The cross section of the dam is shown in Figure 4.12.



**Figure 4.11: Variation of horizontal and vertical displacements
(Clough et. al., 1967)**

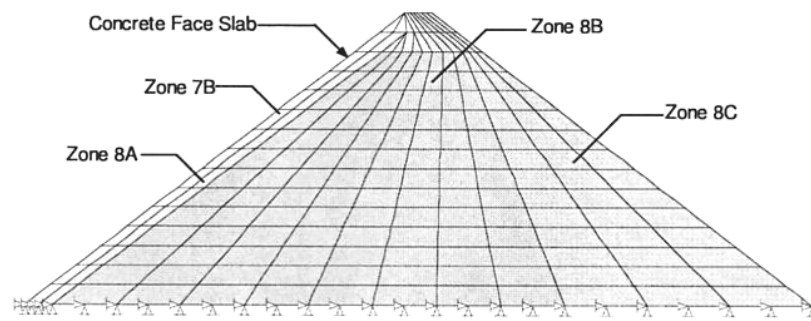


**Figure 4.12: Cross section of Toulnostouc Dam
(Szostak-Chrzanowski and Massiera, 2006)**

The model was analyzed for different foundation conditions. The first model was on hard rock which is also the real case for the Toulnostouc Dam and the second model was on a 60 m high foundation of dense moraine.

The displacements for these two conditions after reservoir filling stage are shown in Figure 4.13. It can be seen that concrete faced rockfill dam (CFRD) on moraine deforms more than CFRD on hard rock.

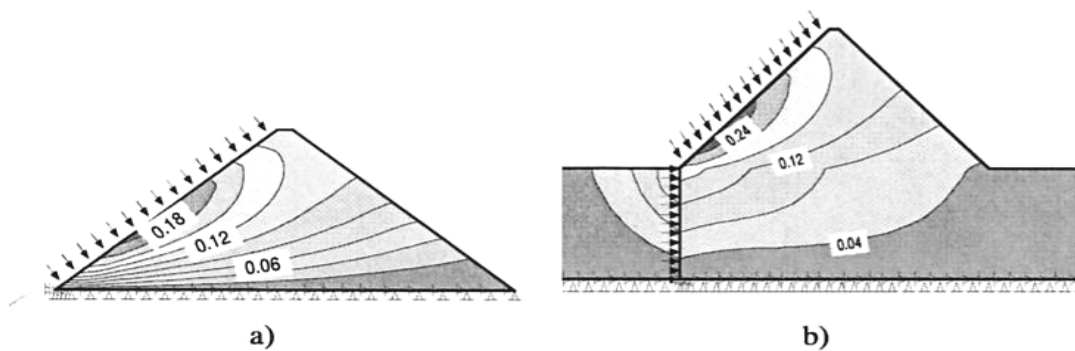


**Figure 4.13: Calculated horizontal displacements (in meters) of the CFRD on
a) rock and b) moraine (Szostak-Chrzanowski and Massiera, 2006)**

4.2.2 Comparison of Two-dimensional and Three-dimensional Finite Element Analysis Results

According to Lefebvre et. al. (1973), two dimensional analysis is preferable than three-dimensional analysis due to its relative simplicity and practicability. However, two dimensional analysis is suitable for embankment dams having smooth valley profiles, recalling that cross-valley arching effect is not considered in plain strain analysis.

Lefebvre et. al. (1973) studied the effect of arching by considering three different slopes of V-shaped valleys, 1:1 (1 horizontal and 1 vertical), 3:1 and 6:1. The dam slopes both in upstream and downstream were (2.5:1) with a height of 49 m for all different valleys. In the analysis linear elastic material properties were used. Also eight construction stage was selected to simulate the real behavior of the dam. It was observed that the magnitudes of the settlements decrease with increasing steepness of the valley slopes. The vertical displacement contours obtained for three valley types are shown in Figure 4.14.

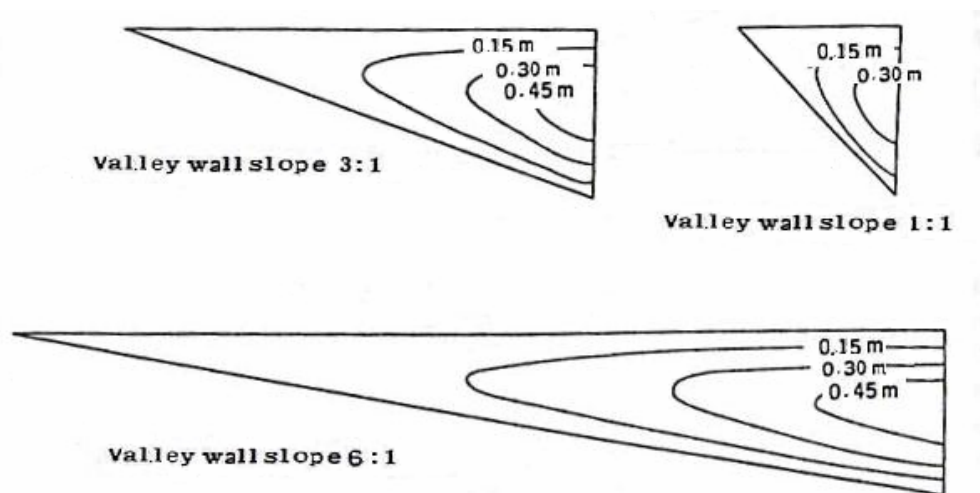


Figure 4.14: Vertical displacement contours (Lefebvre et. al., 1973)

Although the variations are similar for each case, the maximum value is smaller for the steepest valley due to the arching effect. The comparison of plain strain analysis and three-dimensional analysis for transverse section is given with average and variation values at Table 4.2. From the table it can be concluded that, two dimensional analyses give acceptable degree of accuracy for dams with valley slopes of 3:1 or flatter.

Table 4.2: Comparison of plane-strain analysis and three-dimensional analysis (Lefebvre et. al., 1973)

Valley-wall slope	(Plane Strain Values/3-Dimensional Values) 100%					
	1:1		3:1		6:1	
	Avrg.	Var.	Avrg.	Var.	Avrg.	Var.
Max. principal stress, σ_1	113	100-129	102	100-113	101	98-109
Min. principal stress, σ_3	98	79-125	96	81-111	97	88-100
Max. shear stress, τ_{max}	138	108-225	112	100-150	108	100-150
Vertical disp., u_v	136	91-156	106	85-114	100	85-105
Horizontal disp., u_h	268	75-435	120	80-149	105	85-120

Apart from these studies, also Hunter and Fell (2003) examined the effect of valley shape by considering a 100 m height of rockfill dam with the river widths of 20, 50 and 100 m, and abutment slopes of 0, 26.5°, 45°, and 70°. The model was linear elastic with Young's modulus of 100 Mpa and Poisson's ratio of 0.27 where the foundation Young's modulus was 50 Gpa. The results showed that, a "stress reduction factor" should be applied for vertical stresses to the values found by two dimensional analyses in order to take the arching effect into account. These factors are summarized in Table 4.3.

Table 4.3: Stress reduction factors (Hunter and Fell, 2003)

W _r /H ratio (river width to height)	Average abutment slope angle (degrees)	Stress reduction factor (embankment location)			
		Base (0 to 20%)	Mid to low (20 to 40%)	Mid (40 to 60%)	Upper (65% to crest)
0.2	10 to 20	0.93	0.95	0.97	1.0
	20 to 30	0.88	0.92	0.96	0.98
	30 to 40	0.82	0.88	0.94	0.97
	40 to 50	0.74	0.83	0.91	0.96
	50 to 60	0.66	0.76	0.86	0.94
	60 to 70	0.57	0.69	0.82	0.92
0.5	<25	1.0	1.0	1.0	1.0
	25 to 40	0.93	0.95	0.97	1.0
	40 to 50	0.91	0.92	0.95	0.05-1.0
	50 to 60	0.87	0.88	0.93	0.05-1.0
	60 to 70	0.83	0.85	0.90	0.05-1.0
1.0	All slopes	0.95-1.0	0.95-1.0	1.0	1.0

4.2.3 Comparison of Measured and Calculated Settlements of IFRD

The comparison of observed and calculated deformation values is significant in order to assess any unexpected behavior. Although geotechnical parameters can be assessed by laboratory tests or in-situ tests, the fill material may not be homogeneous and these parameters may differ from one site to another. A comparison of observed and calculated data helps to confirm the selected geotechnical parameters.

As mentioned before, nonlinear models reflect the real soil behavior better than other models. Pappadai Dam which is a rockfill dam with impervious bituminous membrane was also modeled by considering non-linear material behavior. The height of the dam is 27 m and calcarenite rockfill (homogeneous dam) was used in the dam body. The downstream and upstream slopes of the dam are 2:1 (horizontal to vertical). The foundation of the dam is stiff clay. The vertical permeability coefficients of the foundation is in the range of $3-6 \times 10^{-11}$ m/s. The horizontal

permeability coefficients are about 3-4 times greater than the vertical ones (Lollino et. al., 2005).

Two-dimensional plane strain analysis was used to analyze the dam performance. Lade's double hardening model was selected to study the dam behavior. The dam was constructed in ten layers which was taken into account during the analyses and the mesh of the dam consisted of quadrilateral elements. The cross section and finite element mesh of the dam are given in Figure 4.15. The experimental data of the foundation was used to assess the model parameters. A thin bituminous membrane was constructed on the upstream face to satisfy the impermeability on the dam body. Elastic model was used for the membrane with a Young's modulus of 10×10^6 kPa and a Poisson's ratio of 0.15 (Lollino et. al., 2005).

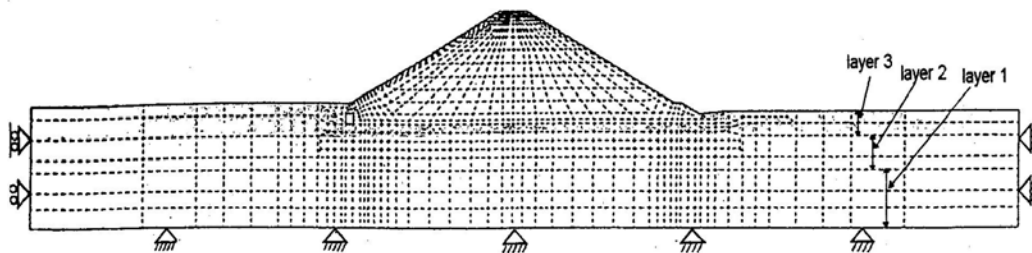


Figure 4.15: Finite element mesh of Pappadai Dam (Lollino et. al., 2005)

The predicted and observed behavior was compared for two stages; i.e. construction and reservoir impoundment. Figure 4.16 shows the comparison of settlements of Pappadai Dam above the foundation level. The observed and predicted values are in a good agreement with each other. The maximum settlement of the dam is observed approximately at the mid-height of the dam as 68 mm.

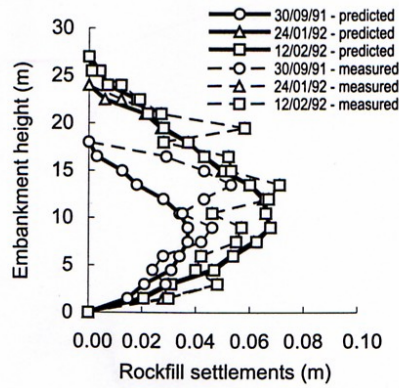


Figure 4.16: Comparison of predicted and measured settlements of Pappadai Dam (Lollino et. al., 2005)

Another study was performed by Özkuzukıran et. al. (2006) for concrete faced rockfill Kürtün Dam, having 133 m height. The dam was constructed in a narrow valley and rest on granodiorite formation. Finite element method was used to assess the dam behavior assuming plane strain conditions. Material model was selected as hardening model. Soil parameters were based on previous studies since laboratory data did not exist. Rock foundation of the dam was assumed to be rigid. Finite element mesh used in the analysis is shown in Figure 4.17. As it can be seen from the figure, mesh consists of triangular elements. Kürtün Dam was analyzed for two conditions; end of construction and reservoir full. Reservoir full condition was analyzed by applying water load on concrete membrane.

Settlement-measuring devices were located in 6 different axes. A comparison of end of construction and reservoir full conditions is given in Table 4.4. From the table it can be seen that observed and calculated settlements for end of construction are close to each other. For reservoir full condition, calculated values are larger than the observed ones. It should noted that this may be due to the unloading-reloading effect (Özkuzukıran et. al., 2006).

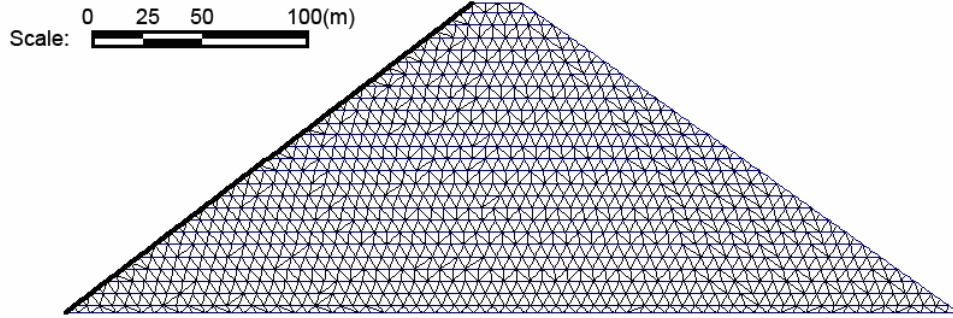


Figure 4.17: Finite element mesh of Kürtün Dam (Özkuzukıran et. al., 2006)

Table 4.4: Comparison of calculated and observed settlements for end of construction and reservoir full condition (Özkuzukıran et. al., 2006)

Axis	Elevation	EOC		RFC	
		Computed Sett. (mm)	Observed Sett. (mm)	Computed Sett. (mm)	Observed Sett. (mm)
A-A	555.00	452	311	433	371
B-B	575.00	680	609	442	384
C-C	555.00	1323	1113	166	44
	575.00	1397	1417	246	173
	600.00	869	836	334	238
D-D	555.00	1553	1460	98	52
	575.00	1838	2019	137	83
	600.00	1592	1592	167	127
	625.00	771	621	170	146
E-E	555.00	1623	1607	65	28
	575.00	1971	2155	87	78
	600.00	1822	1861	103	73
	625.00	1099	717	108	143
F-F	555.00	1491	1313	35	12
	575.00	1712	1669	45	64
	600.00	1360	1462	53	52

4.3 Seepage for Rockfill Dams:

In geotechnical engineering, the flow of water through the soil is one of the fundamental issues. The primary reason for seepage is gravity such as hydraulic head difference between upstream and downstream level.

Seepage of water through porous material's interconnecting voids depends on permeability of the material. Permeability depends on size and shape of soil particles, type of soil and the degree of packing. Coarse soils are more pervious than fine soils. Theoretically, all the soils have some porosity. However, in practice the soils which permit the flow with relative ease is called pervious and soils which permit very little flow is called impervious. Coefficient of permeabilities for textural fractions in soil is given in Table 4.5 (Singh and Varshney, 1995).

Table 4.5: Relative values of soil permeabilities (Singh and Varshney, 1995)

Degree of permeability	Range of coefficient of permeability (k) (cm/s)	Soil Texture
High	$> 10^{-1}$	Medium and coarse gravel
Medium	10^{-1} to 10^{-3}	Fine gravel; coarse, medium and fine sand
Low	10^{-3} to 10^{-5}	Very fine sand, silty sand, loose silt, loess, rock flour
Very low	10^{-5} to 10^{-7}	Dense silt, dense loess, clayey silt, clay
Impermeable	$< 10^{-7}$	Homogeneous clay

4.3.1 Seepage Theory

Seepage flow may be steady or unsteady. At the beginning of the flow seepage will be unsteady and after some time it becomes steady. Seepage flow through soils is defined by Darcy's law:

$$V = -k \cdot i \quad (\text{Equation 4.4})$$

where,

V: the seepage velocity in terms of full soil cross section

i: gradient or rate of loss of head

k: the coefficient of permeability

General governing differential equation for two dimensional seepage is (Seep-W Manual, 2004):

$$\frac{\partial}{\partial x} \left(k_x \cdot \frac{\partial H}{\partial x} \right) + \frac{\partial}{\partial y} \left(k_y \cdot \frac{\partial H}{\partial y} \right) + Q = \frac{\partial \theta}{\partial t} \quad (\text{Equation 4.5})$$

where,

H: total head

k_x : coefficient permeability in x-direction

k_y : coefficient of permeability in y-direction

Q: applied boundary flux

θ : volumetric water content

t: time

This equation states that the change in flows in x and y direction plus the external applied flux is equal to volumetric water content with respect to time. Under steady-state condition, the flux entering and leaving the system is equal all times. As a result, right side of the equation becomes zero (Seep-W Manual, 2004).

4.3.2 Seepage through Rockfill Dams

Measuring displacements, total stresses, pore-water pressures and seepage are important for characterizing the dam's overall behavior. Pagano et. al (2006) studied Polverina Dam which has a height of 27.5 m. It is a rockfill dam with impervious earth core. The foundation of the dam is fluvial deposits with a depth of 20 m. Therefore, water-tightness inside the foundation is provided by a concrete cutoff

wall with a thickness of 0.5 m. The cross section of the dam is shown in Figure 4.18. Piezometer measurements, given in Figure 4.19, increase with the construction as the saturation takes place with overburden material. After the construction, pore pressures decrease during the consolidation process. During the first impoundment, surprisingly pore pressure changes at downstream piezometer are more significant than the upstream and central piezometers. However some months after the impoundment the measured values show more typical trend such as the pore pressures decrease from upstream to downstream as expected.

Under undrained conditions, pore pressure changes are directly affected by total stress increments. Mechanical nonhomogeneities may cause total stress discontinuities. Therefore, nonhomogeneities in the soil affects pore pressure distribution much. This is the reason for the unusual behavior of the Polverina Dam.

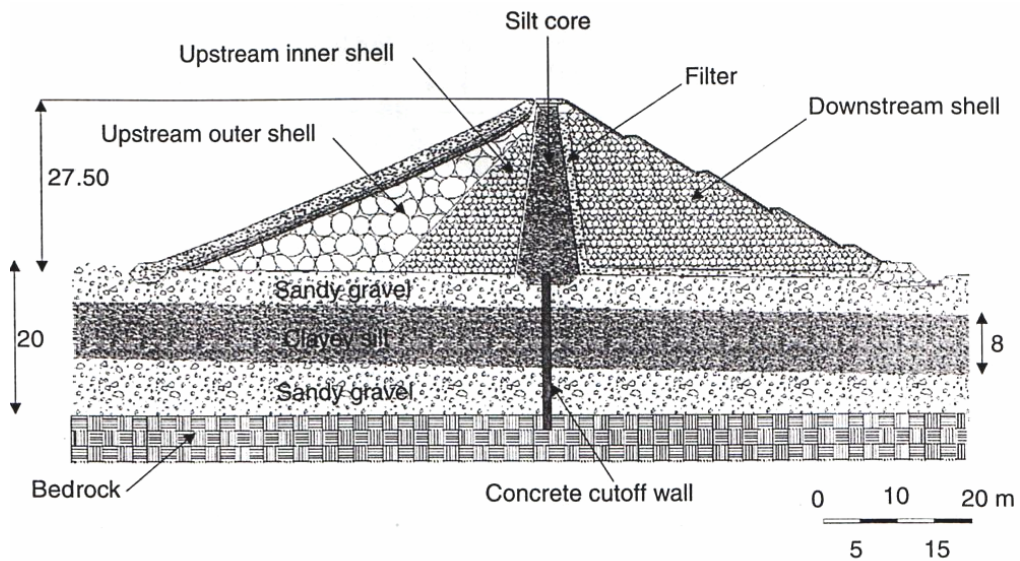


**Figure 4.18: Cross section of Polverina Dam with material zones
(Pagano et. al., 2006)**

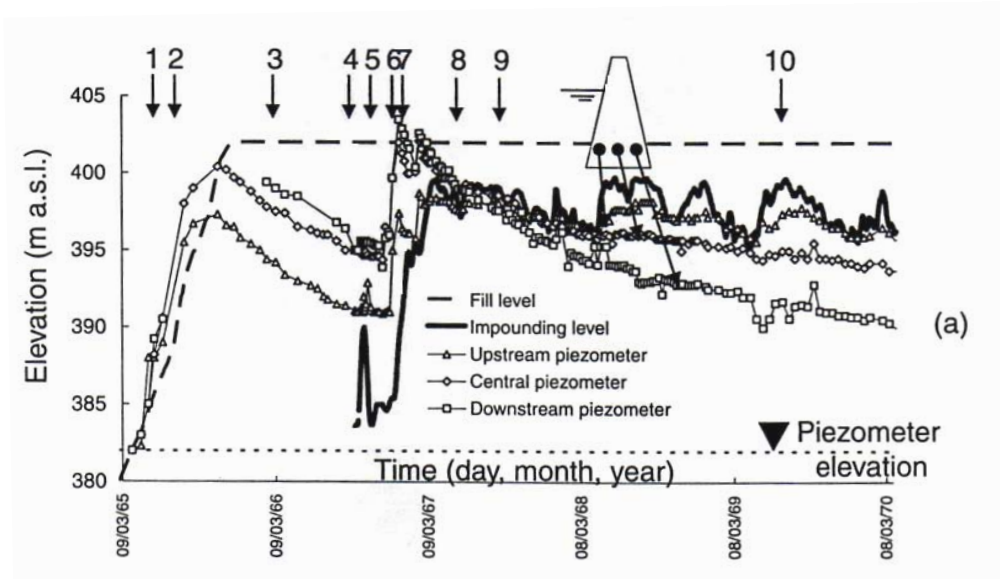


Figure 4.19: Piezometer measurements of Polverina Dam (Pagano et. al., 2006)

4.3.3 Finite Element Model for Steady-State Seepage

Kalkani and Michali (1984) studied on finite element model for steady-state seepage. In this study, an earth dam with an impervious core, and its alluvial foundation with an impervious cutoff was used as a model. The earth dam is approximately 20 m high, consists of impermeable clay core, transition filters and sand-gravel shells. Alluvial fill beneath the dam is 20 m deep with the horizontal permeability (k_x) of 0.001 m/s. The rock strata below the alluvium is completely impermeable. Impermeable cutoff wall thickness is 0.8 m designed to reduce the flow.

In analyses, two different cases were examined. Case 1 represents the flow through the foundation only (simplified flow) and Case 2 represents the flow through the foundation and the dam body. Ground water potential is 70 m for upstream and 52 m for downstream for both cases. The analyses results for Case 1 and Case 2 with $k_x/k_z = 1$ and cutoff wall depth is equal to 50% of the foundation depth is shown in Figure 4.20 and Figure 4.21, respectively.

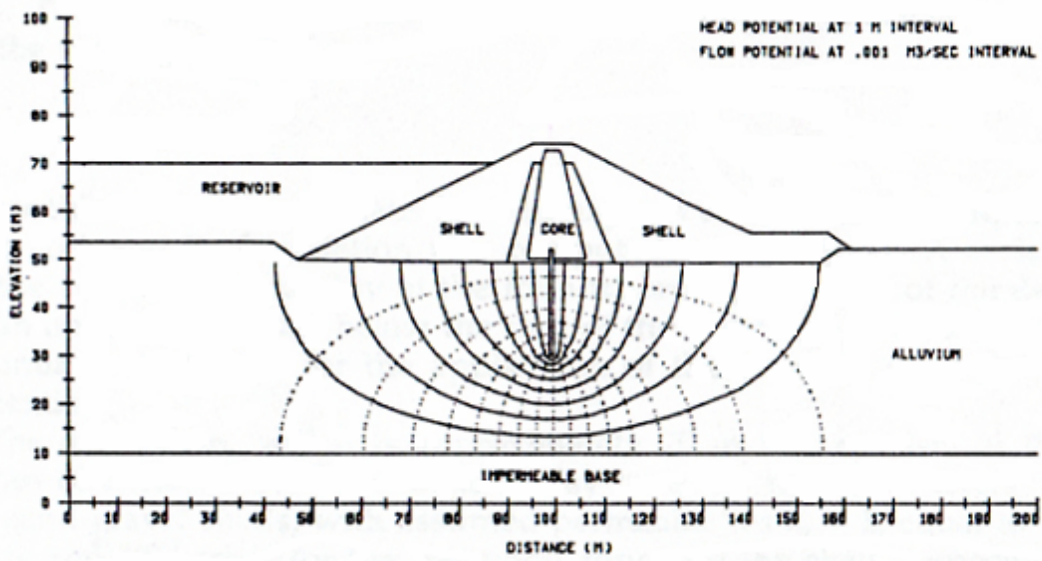


Figure 4.20: Steady-state seepage flow net for case 1
(Kalkani and Michali, 1984)

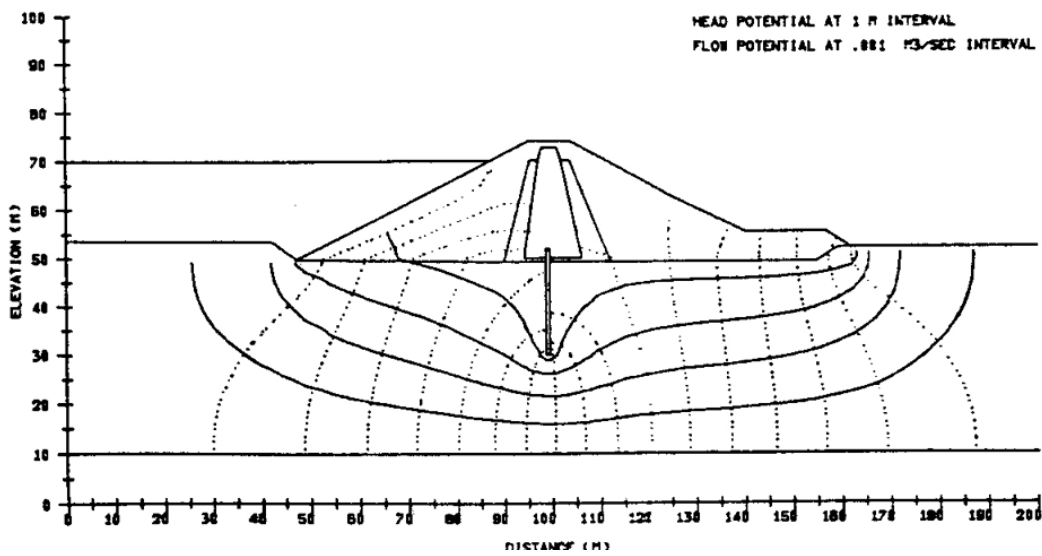


Figure 4.21: Steady-state seepage flow net for case 2
(Kalkani and Michali, 1984)

CHAPTER 5

DEFORMATION AND SEEPAGE ANALYSES OF MURATLI DAM

5.1 General Information about Muratlı Dam:

Muratlı Dam is the first asphalt faced rockfill dam in Turkey and it is located in East Black Sea Region on Çoruh River. The distance between the dam site and Georgia border is approximately 100 m. It is 2 km away from the Muratlı village on the upstream side, and 17 km away from Borçka town on the downstream side. Project aims energy production and overflowing protection. Energy production capacity of the dam is 115 MW and annual generation is 44.12 GWh. Height of the dam is 42 m from the river bed and the slopes of the dam is 2:1 (H:V) for both upstream and downstream sides. Volume of the dam body is 1,981 million m³ and crest length of the dam is 280 m.

Although construction activities began on 01.09.1999, construction of the dam body was started at 26.01.2003 and completed at 17.12.2004. Following the construction of dam body, impervious face placement started after three months of waiting period for the major part of the settlements to be completed to avoid the cracking on the impervious face. This delaying time is less than that of Kürtün Dam (Özkuzukıran et. al., 2006) due to its smaller height and stronger fill material. Reservoir filling was started at 14.03.2005 and the reservoir was filled step by step in 30 days.

Muratlı Dam has asphalt impervious face with 36 cm thickness to satisfy the impermeability. This technique, applied mainly on medium height dams, decreases the cost of the project by considerable amount. Asphalt face provides excellent

water-tightness, durability and flexibility (Singh and Varshney, 1995). A view of the completed dam is given in Figure 5.1.



Figure 5.1: View of Murath Dam

Since the basic geological formation under the dam is alluvium, cut-off wall is constructed down to the rock surface with a maximum depth of 60 m. Cut-off wall is made from impermeable plastic concrete and has compatible deformability with the subsoil (alluvium). Main rock beneath the subsoil is agglomerate and lithic-andesite tuff which is hard. The cross section of the dam is given in Figure 5.2 with material zoning. The legend for the materials and detailed information about the main zones of the dam are presented in Table 5.1.

5.2 Instrumentation in Murathl Dam:

Murathl Dam is heavily instrumented to observe the behavior of the dam. The instruments used in the dam body can be listed as:

- **Inclinometers (IC):** Measure horizontal and vertical deformations in dam body and subsoil (alluvium).
- **Fill-extensometers (EW):** Measure horizontal and vertical deformations behind the asphalt face, vertical deformations at upstream and downstream of cutoff wall and horizontal deformations along the dam body.
- **Earthcells (EC):** Measure earth pressures in dam body.
- **Piezometers (PW):** Measure excess pore water pressures to check the impermeability of cutoff wall.

In the dam body and cofferdam, 48 fill-extensometers, 4 inclinometers, 51 piezometers and 34 earthcells are placed. These instruments are located at two different cross sections. Figure 5.3 and Figure 5.4 shows the fill-extensometers at cross sections A1 (0+200 Km) and A2 (0+300 Km), respectively. Figure 5.5 and Figure 5.6 shows the piezometers, inclinometers and earthcells at cross sections A1 and A2, respectively. The longitudinal section of the Murathl Dam with locations of sections and instruments is shown in Figure 5.7.

Table 5.1: Materials used in the construction of Murath Dam

Zone	Type	Max. Particle Size	Thickness of Layer (m)	Compaction
1	River Alluvium	40	0.6	6 passes with 10 t vibratory roller
2A	River Alluvium or Rockfill (fine material)	20	0.4	4 passes with 10 t vibratory roller
2B	River Alluvium or Rockfill (coarse material)	30	0.6	4 passes with 10 t vibratory roller
3A	Rock Material (Type 1)	60	1	6 passes with 10 t vibratory roller
3B	Rock Material (Type 2)	80	1	4 passes with 10 t vibratory roller
3C	Random Rockfill	60	1.2	2 passes with 10 t vibratory roller
4	Impervious Material	-	0.3	-
5	Filter Material	20	0.4	4 passes with 10 t vibratory roller
6	Riprap	30-100	-	-
7	Surface Protection Layer	10	0.4	4 passes with 10 t vibratory roller

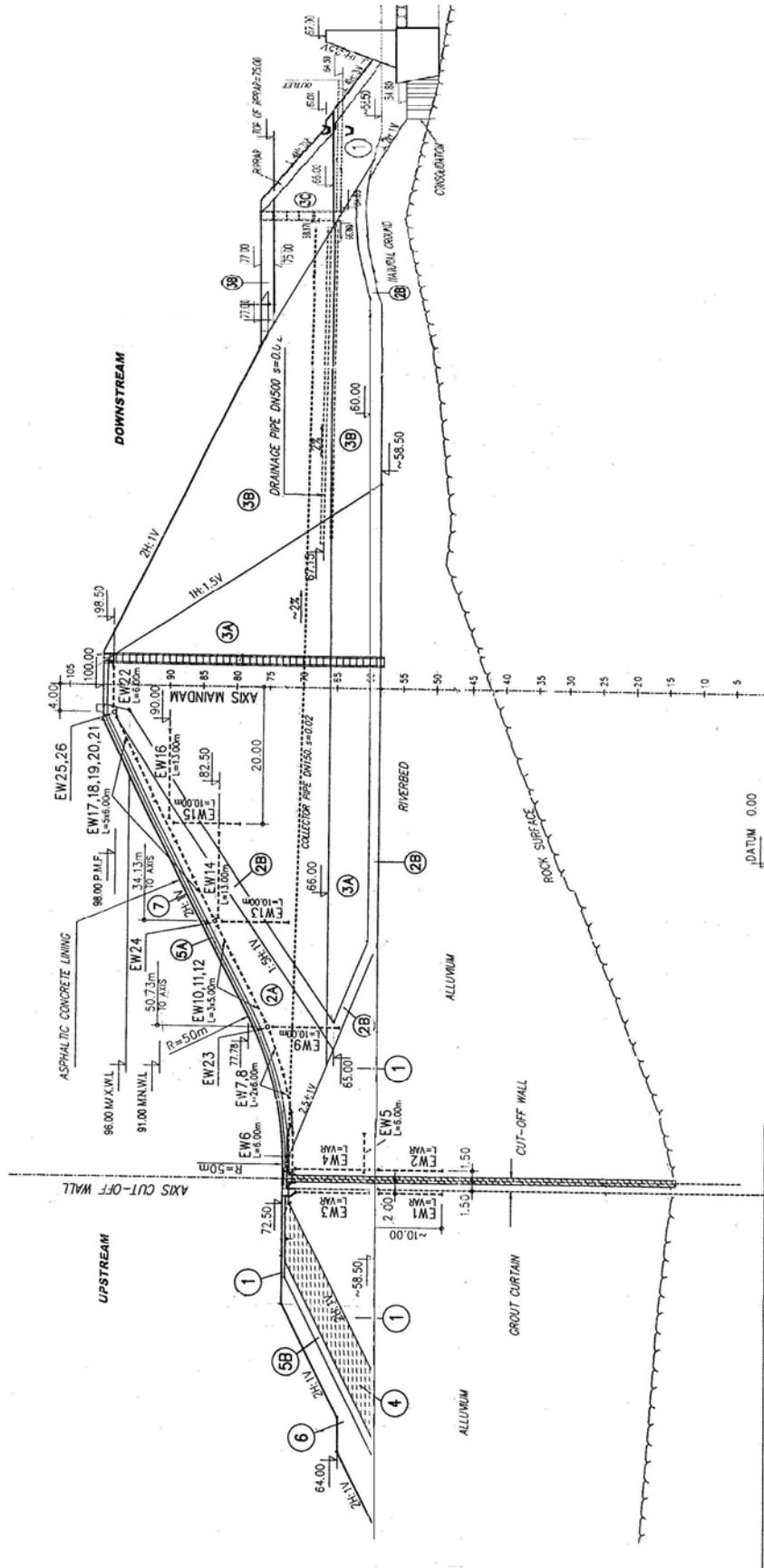


Figure 5.4: Locations of fill-extensometers at section A2 (dimensions are in meters)

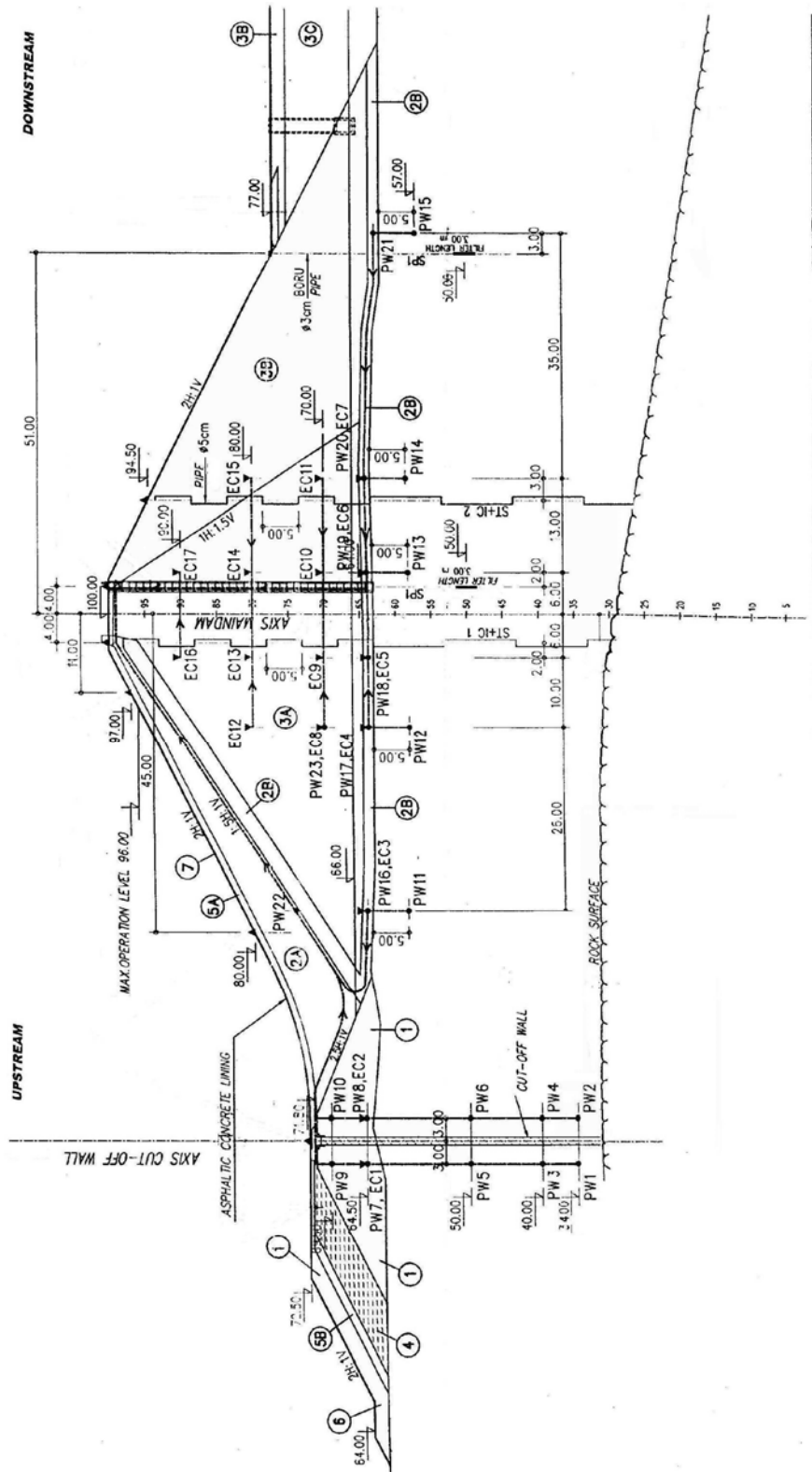


Figure 5.5: Locations of piezometers, inclinometers and earthcells at section A1
(dimensions are in meters)

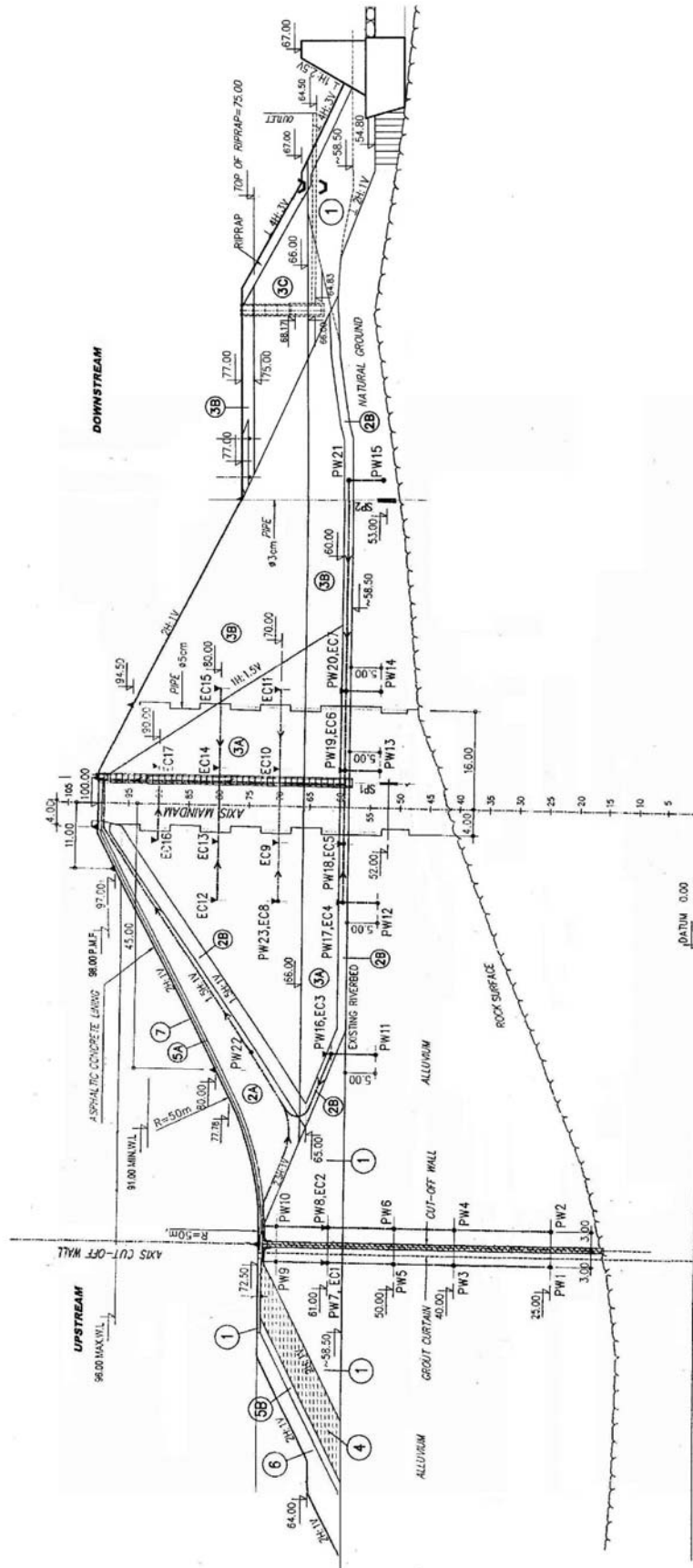


Figure 5.6: Locations of piezometers, inclinometers and earthcells at section A2
 (dimensions are in meters)

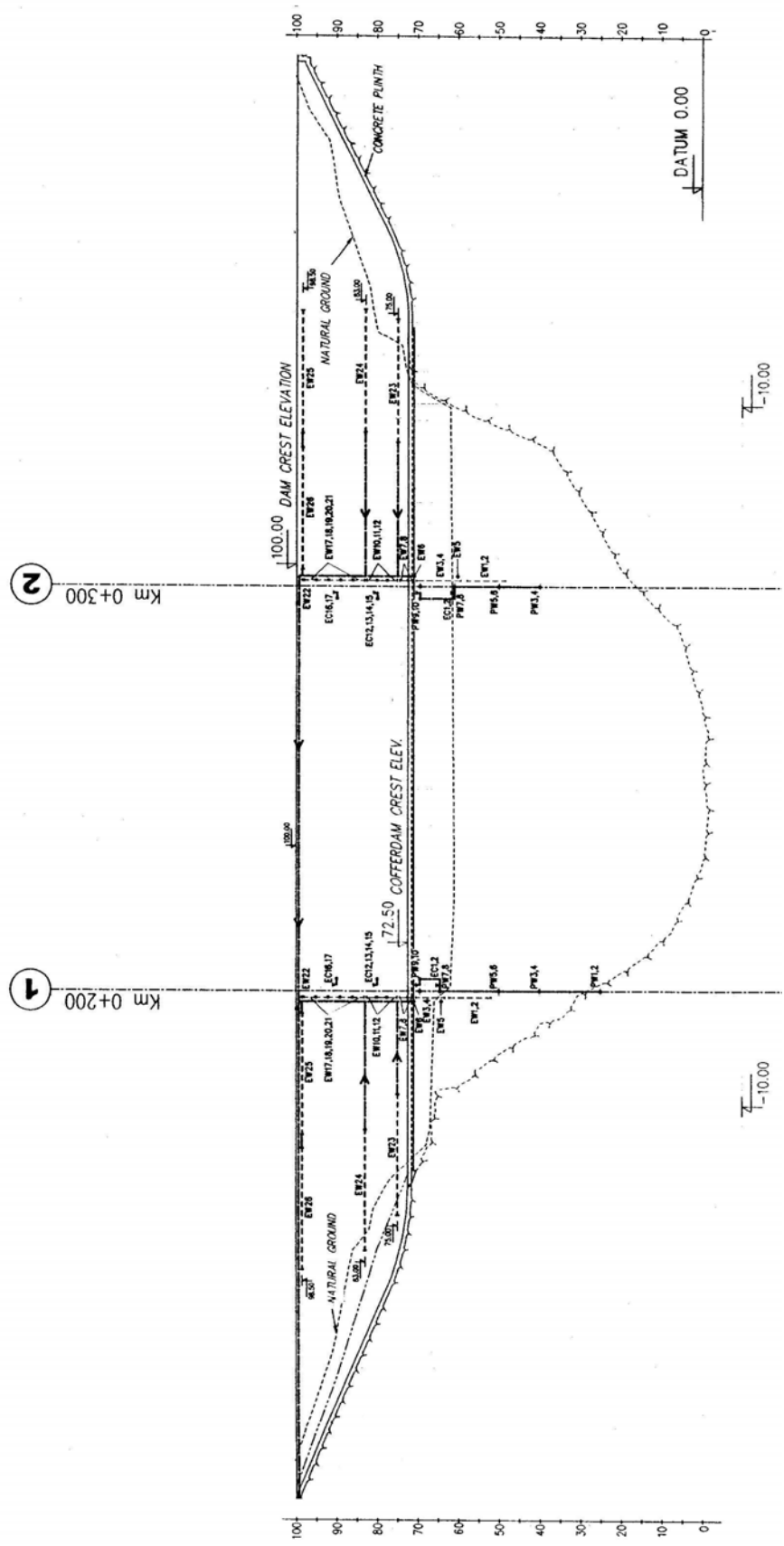


Figure 5.7: Longitudinal section of Murathi Dam with the instrument locations

5.2.1 Inclinometer

Inclinometer measures the lateral and vertical deformation of soil and rock to determine the stability of dams. Inclinometer system includes a probe, cable reel and PDA which allows easy connection between most office systems and applications. The waterproof and stainless steel probe with guide wheels measures the deformation. Then, cable which is waterproof and marked at half meter intervals carries the electrical signals between the probe and the readout. Stretching of the cable is minimized by a stainless steel core. Readings are saved by PDA. Common measurement range of the probe is $\pm 30^\circ$ and the system accuracy is ± 2 mm over 25 m with operating temperature of -20°C to $+50^\circ\text{C}$. An illustration of the inclinometer is given in Figure 5.8 (Roctest Telemac Instrumentation Manual, 2000).



Figure 5.8: Inclinometer

5.2.2 Fill-extensometer

Fill-extensometer measures longitudinal displacement between two points in fill. The system consists of telescopic outer PVC pipe fitted with two end flanges and an inner stainless steel rod. Both ends of the rod attached to a flange and one end of the rod attached to a displacement sensor. Readings can be obtained by a signal cable

which is attached to the sensor. When a displacement occurs in a fill, the telescoping outer pipe also moves with soil, and as a result compression or tension occurs in the rod. It is generally installed horizontally in trenches and sometimes vertically in boreholes. The standard length of the fill-extensometer is between 3 - 30 meters. The range of the fill-extensometer is 50, 100, 150, 200 mm with operating temperature -20 to $+80$ °C. An illustration and a schematic model of a fill-extensometer are shown in Figures 5.9 and 5.10, respectively (Roctest Telemac Instrumentation Manual, 2000).



Figure 5.9: Fill-extensometer

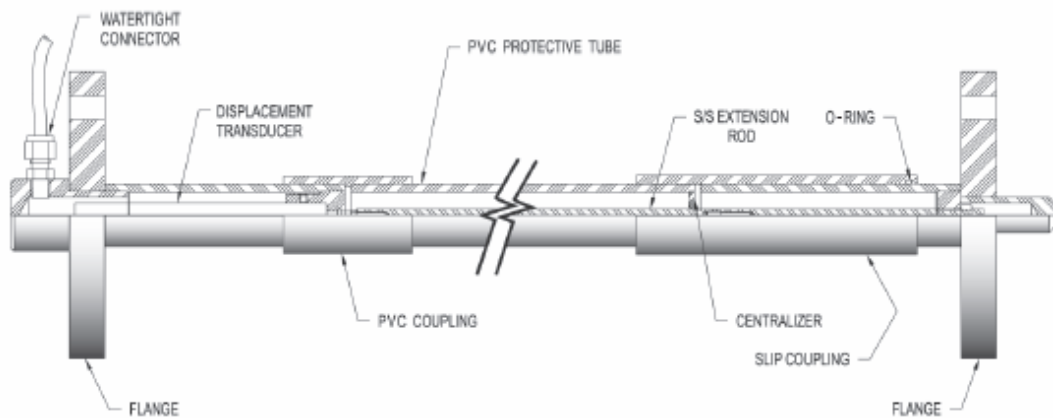


Figure 5.10: Schematic model of a fill-extensometer

5.2.3 Earthcell

Earthcell measures the total stress and its direction in embankments. It consists of two plates which are welded together around periphery and filled with de-aired oil. This pad is connected to a pressure transducer by a steel tube. When a variation from load change occurs in oil pressure, transducer records the change. It is installed or embedded in contact with soils. It is only sensible to normal stress. The stiffness of the earthcell is very high due to the small quantity of oil and high stiffness of the transducer. The small amount of oil used in the pad also minimizes the effect of the temperature. Although it has very high stiffness, it satisfies the flexibility which is necessary for the equality of oil pressure with the soil contact pressure on the pad due to its peripheral groove. Plates of the earthcell can be circular or rectangular, both of which are shown in Figure 5.11 (Roctest Telemac Instrumentation Manual, 2000).



Figure 5.11: Earthcell

5.2.4 Piezometer

Piezometer, which is pressure transducer, measures pore-water pressure and piezometric level. It consists of a vibrating wire sensing element enclosed in a protective steel housing. Its vibration period is measured by an electromagnetic coil. The output is a frequency signal which is transmitted over long distances. The end

of the piezometer which is installed in boreholes is covered with an air entry filter to protect sensing element from solid particles. In Figures 5.12 and 5.13 different models of piezometers and a schematic model of a piezometer are shown, respectively (Roctest Telemac Instrumentation Manual, 2000).



Figure 5.12: Piezometer models

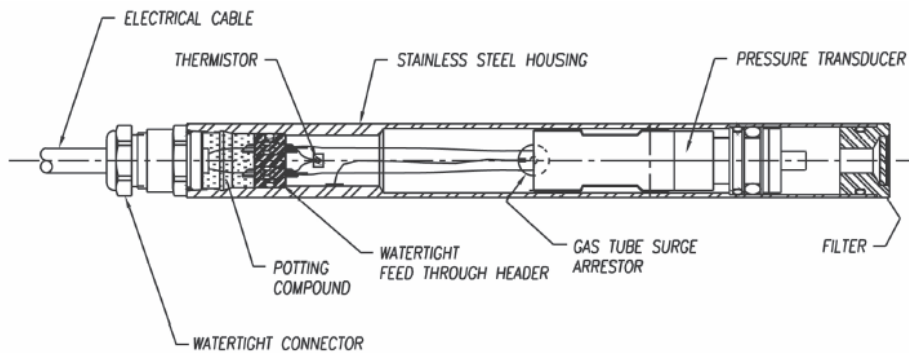


Figure 5.13: Schematic model of a piezometer

5.3 Stability Analyses of Muratlı Dam:

5.3.1 Material Model and Parameters

As mentioned before, rockfill material is nonlinear, stress dependent and inelastic. In previous studies, generally hyperbolic model was used to represent these properties of the rockfill. However, recently hardening model which is enhanced form of hyperbolic model is used in studies such as the case of Kürtün Dam (Özkuzukıran et. al., 2006). Hardening model is based on plastic theory rather than elastic theory (Schanz et. al., 1999).

In this study, Plaxis v7.2 software is used with hardening model to reflect the real soil behavior of Muratlı Dam. Parameters for hardening model are normally determined by triaxial test machines. However, testing rockfill is difficult due to the big size of the particles. Therefore, on the basis of previous studies, a starting point is defined and back analyses are done to find the best fit.

It is planned to use inclinometer values to find the best fit parameters for Muratlı Dam. However, misreading of the inclinometer measurements make it impossible. Therefore, fill-extensometer measurements are used to define shear strength characteristics of the materials. Fill-extensometers are located at four different directions in the dam body (Figure 5.3 and 5.4). Horizontal and vertical ones are placed during the construction of the dam. In each cross section, there are 7 vertical fill-extensometers and 4 horizontal fill-extensometers under the asphalt face and at upstream and downstream side of the cutoff wall. Fill-extensometers parallel and vertical to the face are placed before the asphalt face construction. Therefore mainly first two types of fill-extensometers are used for the analyses. Readings of vertical extensometers are given in Table 5.2.

Table 5.2: Recorded vertical fill-extensometer values for section A1 (0+200 Km) and A2 (0+300Km)

A1 Cross Section				A2 Cross Section			
Instrument	X* (m)	Elevation (m)	Observed Value (mm)	Instrument	X* (m)	Elevation (m)	Observed Value (mm)
EW15	99.09	89.35	-10.70	EW15	106.00	89.40	-16.85
	99.09	79.35			106.00	79.40	
EW13	84.18	82.60	-	EW13	91.37	82.55	-23.06
	84.18	72.60			91.37	72.55	
EW9	68.13	74.89	-16.23	EW9	74.88	75.00	-
	68.13	64.89			74.88	65.00	
EW4	46.74	71.00	-1.75	EW4	53.43	71.00	-1.93
	46.74	64.00			53.43	64.00	
EW3	43.47	71.00	-1.04	EW3	50.10	71.00	-0.34
	43.47	64.00			50.10	64.00	
EW2	46.74	61.50	-2.30	EW2	53.43	61.50	-0.51
	46.74	51.50			53.43	51.50	
EW1	43.47	61.07	-0.43	EW1	50.10	61.50	-0.42
	43.47	51.07			50.10	51.50	

***Distance from the upstream toe of the cofferdam**

Deformation of 42 m high Muratlı Dam is considerably smaller than the deformations of the impervious faced rockfill dams; Shiroro Dam (Bodtman and Wyatt, 1985), Foz do Areia Dam (Saboya and Byrne, 1993) and Kürtün Dam (Özkuzukıran et. al., 2006). In the light of this information, hardening model material parameters of Cethana Dam which has a height of 110 m with the recorded maximum settlement of 450 mm is taken into account for the preliminary analyses. A study on behavior of Cethana Dam was made by Khalid et. al. in 1990. Hyperbolic stress strain parameters of Cethana Dam is based on the analysis of Tehri Dam (Khalid et. al., 1990, after Sharma, 1976) since laboratory test data was not available. The hyperbolic parameters for rockfill used in the analysis of Cethana Dam are provided in Table 5.3.

**Table 5.3: Hyperbolic stress strain parameters for rockfill material
(Khalid et. al., 1990)**

Parameters	Values
Unit weight, γ (kN/m ³)	20
Cohesion, c (kN/m ³)	-
Friction Angle, ϕ (°)	38
Modulus number, K	2500
Modulus exponent, n	0.25
Failure ratio, R_f	0.76

Using the modulus number, K , given in the table, E_{50}^{ref} can be obtained from the expression, $E_{50}^{ref} \approx 50K_E$ (Özkuzukiran et. al, 2006). Although “ c ” value is “0” both for rockfill and alluvium, it is taken as “1 kPa” in order to provide the stability of the numerical analyses. Zone 2A, 2B, 5, 6 and 7 are modeled as a single transition material since their properties are similar to each other. Zone 4 is a small zone in impervious layer of the cofferdam and the parameters of transition zone are assigned for this zone. Previous studies on Da’ao Dam (Xing et. al., 2006) and Oroville Dam (Kulhawy and Duncan, 1972) show that transition zone model parameters can be taken close to main rockfill. Therefore, transition zone model parameters similar to the main rockfill parameters used in the analyses.

From the experiments, it can also be seen that subsoil is an alluvium with boulders without silt layers. Parameters of subsoil are determined from test results; $\gamma = 22$ kN/m³, $c = 0$ kN/m³ and $\phi = 35^\circ$. Hardening parameters are assessed from the back analyses. Rock beneath the subsoil is assumed as rigid and parameters for rock are selected according to this assumption.

Two beam elements used in the model; the cutoff wall and the asphalt face. Elastic material behavior is selected for both of them. Cutoff wall is designed to deform compatible with the subsoil. Generally, cutoff wall has a modulus of elasticity of

2.5-5 times of the subsoil modulus. Asphalt face material properties are taken as 10×10^6 kPa for Young's modulus and 0.15 for Poisson's ratio from the studies of Lollino et. al. (2005).

5.3.2 Specifications for the Analyses

Loading conditions at Muratlı Dam can be separated into two main parts; first one is end of construction (EOC) and the second one is reservoir impounding (RI). In the first case, the dam deformed under its own weight and in the second case, the deformation is due to the application of water load on the impervious face.

Generally, the maximum cross section is selected for the analyses. Since maximum section deforms more than other sections, it is the most critical one. Muratlı Dam has two instrumented cross sections; A1 (0+200) and A2 (0+300). In this study, for EOC both cross sections are studied. However for RI analyses, cross section A1 is used only, since the measurements are more reliable than A2.

As mentioned in previous sections, stage construction has a significant effect on stress distributions, horizontal deformations and especially on vertical deformations (Clough et. al., 1967). Therefore, the model used in the analyses is carried out in stages to reflect the real construction condition. The layer thicknesses during the stage analyses are taken as 4 - 5 m depending on the construction schedule.

Analyses of Muratlı Dam are done with 15-node elements. The finite element mesh used in the analyses for cross section A1 is given in Figure 5.14.

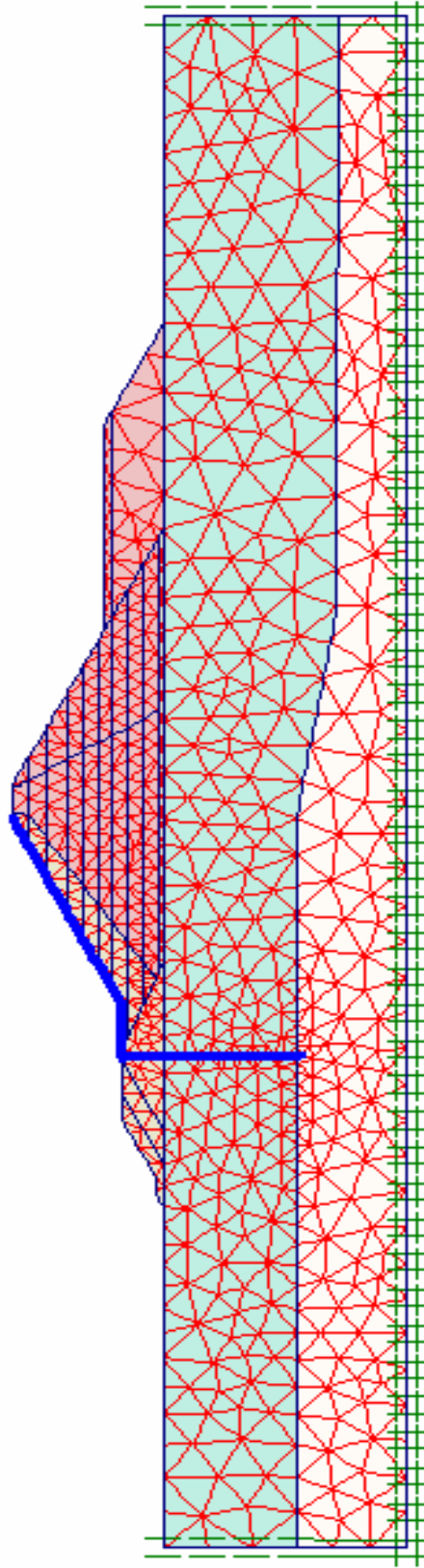


Figure 5.14: Finite element mesh used in the analyses

5.3.3 Preliminary Analyses

As it is mentioned before, stress strain parameters for rockfill are estimated by taking the parameters used for Cethana Dam into account for the preliminary analyses. In these analyses, dam is assumed to consist of single material with the parameters given in Table 5.3. At the end of these analyses, it is seen that the dam behaves stiffer than the observed behavior. As a result, E_{50}^{ref} value is decreased until the calculated deformations converge to the observed ones.

Following single material analyses for a range of E_{50}^{ref} value, effect of the other hardening parameters are examined by changing only one parameter for each analysis. It is observed that, “ R_f ” does not have any significant effect on the relative displacement between two points and it is taken as 0.75 (same with Cethana Dam) for all materials and when m value is increased, deformations decrease.

After the preliminary analyses, the range for the stress strain parameters for each material is selected (Table 5.4). Friction angle values are taken from Verbundplan Final Design Review Report, 2001. Dilatancy angle (Ψ) can be estimated by the formula $\psi \approx \phi - 30^\circ$ and E_{oed}^{ref} is taken equal to the E_{50}^{ref} (Plaxis Material Manual, 2004).

Rockfill of Muratlı Dam contains three types of rock; 3A, 3B and 3C (Figure 5.2). In the analyses these zones are assumed to have same material constants since there is no enough test data on rock materials and the analyses are compared with the surface measurements. It is seen that zones 3B and 3C do not have a significant effect on surface deformations as observed during the analysis of Kürtün Dam (Özkuzukıran et. al., 2006).

Table 5.4: Range of stress strain parameters for the model

Material	c_{ref} (kPa)	ϕ ($^{\circ}$)	E_{50}^{ref} (kPa)	m	R_f	γ (kN/m ³)
Rockfill	1.0	35-40	60000-80000	0-0.3	0.75	17-20
Alluvium	1.0	32-38	30000-50000	0-0.3	0.75	17-22
Subsoil	1.0	35	200000-400000	0-0.3	0.75	22

5.3.4 End of Construction Analyses

Different combinations of the parameters are examined for both cross sections and parameters which are the best fit with the observed measurements are summarized in Table 5.5. E_{50}^{ref} and m are selected by considering the fill-extensometer measurements and γ is taken from earthcell measurements. Elasticity of the cutoff wall directly affects the calculated vertical displacements located near the cutoff wall. From progressive analyses, elasticity of the cutoff wall is decided to be 4 times greater than that of subsoil which is equal to 1200 MPa and 1400 MPa for sections A1 and A2, respectively.

Table 5.5: Stress strain parameters for cross sections A1 and A2

Material	ϕ ($^{\circ}$)		E_{50}^{ref} (kPa)		m		γ (kN/m ³)	
	A1	A2	A1	A2	A1	A2	A1	A2
Rockfill	40	35	70000	60000	0.3	0.3	19	18
Alluvium	38	32	32500	35000	0.3	0.3	20	19
Subsoil	35	35	300000	350000	0.3	0.3	22	22

5.3.4.1 Vertical Deformations

Comparison of calculated and observed vertical deformations using the best-fit parameters for cross sections A1 and A2 is summarized in Table 5.6 and Table 5.7, respectively. In these tables, “+” value means tension and “-” value means compression. Location of the fill-extensometers for cross sections A1 and A2 can be seen in Figure 5.3 and Figure 5.4, respectively. It can be seen that measurements made by EW9 and EW15 at section A1 and EW13 and EW15 at section A2 located in the dam body are in good agreement with calculations. EW13 at A1 and EW9 at A2 are ignored since the observed values are inconsistent and unreliable. From the Tables 5.6 and 5.7 it can be seen that measurements of EW1 and EW3 located at upstream side of the cutoff wall and at the same distance from the cutoff are also in good agreement with calculated values. However, the same can not be said for EW2 and EW4 located at downstream side of the cutoff wall. The difference between observed and calculated values at these locations may be attributed to the boulders in the subsoil having dimensions up to 2~3 m.

Two inclinometers are located at each section. IC1 is located 4 m upstream of dam axis and IC2 is located 16 m downstream of dam axis. Comparison of the observed and calculated settlements could not be done due to errors made during readings.

Calculated settlements at locations IC1 and IC2 in section A1 are given in Figure 5.15. In the figure, elevations between 0 and 30 m correspond to rock, elevations from 30 m to 62 m correspond to subsoil and elevations from 62 m to 100 m correspond to the dam body. In the dam body, maximum settlement is observed at about mid-height of the dam as 110 mm. It can also be said that rock beneath the subsoil behaves as an elastic body, and the settlement in rock is found to be approximately 8 mm. At the top of the subsoil, settlement is calculated as 45 mm.

An inclinometer plot for section A2 is given in Figure 5.16. Maximum settlement is about 145 mm and occurred at mid-height of the dam body. From Figure 5.16, it can be seen that deformations of A2 section is greater than A1 section as expected.

However, behavior of the dam body is similar in both sections. Settlement found at IC1 location is greater than that of IC2 location for both sections, because location of IC1 is closer to the main dam axis.

Table 5.6: Comparison of calculated and observed vertical deformation values for cross section A1

Inst.	X* (m)	Elevation (m)	Calculated Deform. (mm)	Observed Deform. (mm)	Difference (%)
EW 15	99.09	89.35 - 79.35	-11.31	-10.70	0.61
EW 13	84.18	82.6 - 72.6	-24.45	-	-
EW 9	68.13	74.89 - 64.89	-18.07	-16.23	1.84
EW 4	46.74	71 - 64	-4.87	-1.75	3.12
EW 3	43.47	71 - 64	-1.50	-1.04	0.46
EW 2	46.74	61.5 - 51.5	-1.04	-2.30	1.26
EW 1	43.47	61.07 - 51.07	-0.65	-0.43	0.22

* Distance from the upstream toe of the cofferdam

Table 5.7: Comparison of calculated and observed vertical deformation values for cross section A2

Inst.	X* (m)	Elevation (m)	Calculated Deform. (mm)	Observed Deform. (mm)	Difference (mm)
EW 15	106.00	89.40 - 79.40	-13.97	-16.85	2.28
EW 13	91.37	82.55 - 72.55	-24.77	-23.06	1.71
EW 9	74.88	75.00 - 65.00	-18.93	-	-
EW 4	53.43	71.00 - 64.00	-3.19	-1.93	1.26
EW 3	50.10	71.00 - 64.00	-0.91	-0.34	0.57
EW 2	53.43	61.50 - 51.50	-1.76	-0.51	1.25
EW 1	50.10	61.50 - 51.50	-0.80	-0.42	0.38

*Distance from the upstream toe of the cofferdam

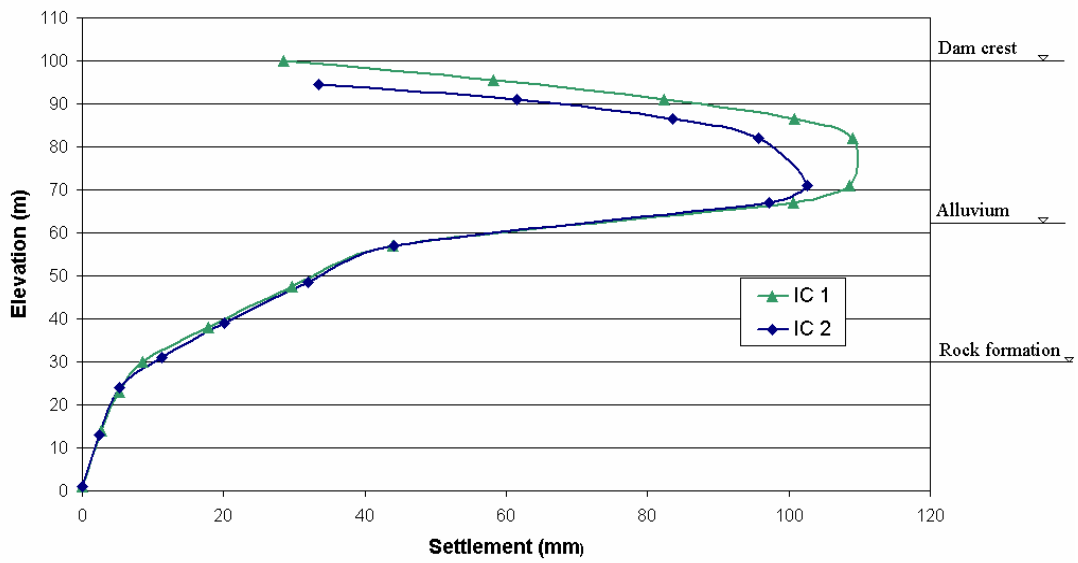


Figure 5.15: Calculated vertical deformations at IC1 and IC2 for section A1

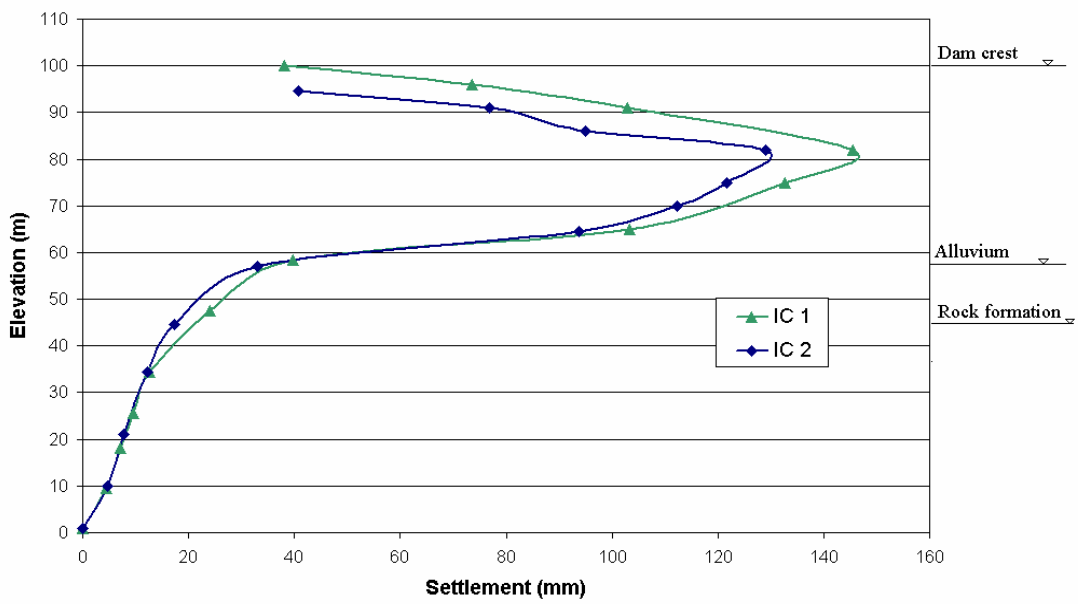


Figure 5.16: Calculated vertical deformations at IC1 and IC2 for section A2

5.3.4.2 Horizontal Deformations

After the evaluation of settlements, section A1 is used to investigate the behavior of Muratlı Dam since measurement results are more consistent at this section. Comparison of computed and observed horizontal deformations for cross section A1 is given in Table 5.8. It can be seen from the table that the agreement is quite satisfactory for EW5 and EW22. On the other hand, for EW16 for which analysis results indicate tension, compression is observed.

Table 5.8: Comparison of calculated and observed horizontal deformation values for cross section A1

Inst.	X* (m)	Elevation (m)	Calculated (mm)	Observed (mm)	Difference (mm)
EW 22	115.15-121.15	99.11	0.48	0.68	0.20
EW 16	99.00-112.00	89.93	0.93	-1.48	2.41
EW 14	84.14-97.14	82.61	2.55	4.52	1.97
EW 5	53.79-59.79	64.34	-1.38	-1.34	0.04

***Distance from the upstream toe of the cofferdam**

Calculated horizontal deformations at inclinometer locations are given in Figure 5.17. Although top part of the dam body deforms towards upstream direction, the rest of the dam body and subsoil deforms towards downstream direction. This may be due to the unsymmetrical geometry of the dam and material. Horizontal deformations occur in rock beneath the subsoil can be ignored. From figure, it can also be said that maximum deformation occurs at the crest and the value of the maximum horizontal deflection is 10 mm.

Figure 5.18 shows the observed and calculated deformations for end of construction condition. It is seen that, most of the points are within the region bounded by the lines having slopes 2:1 and 1:2 (H:V).

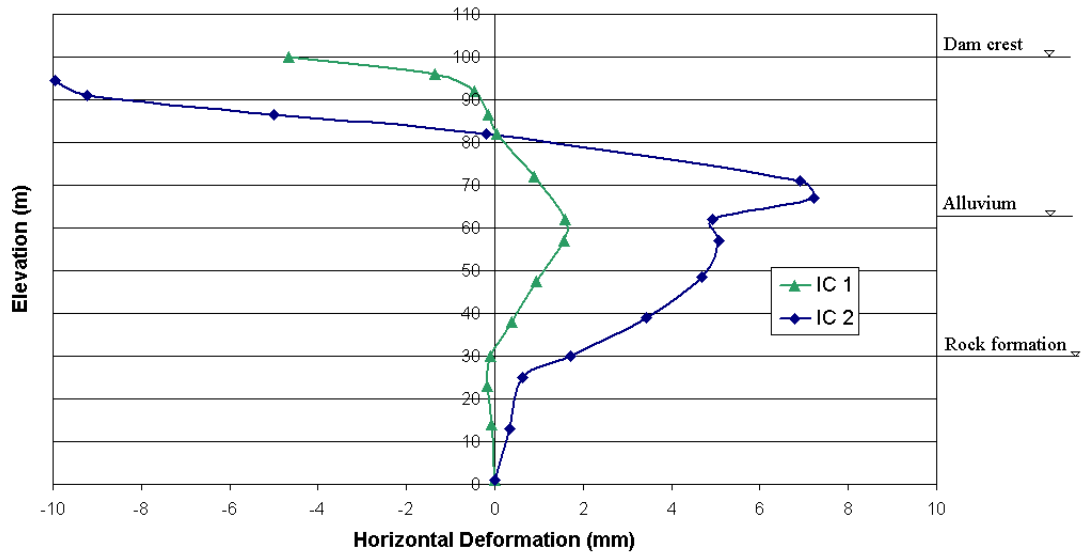


Figure 5.17: Calculated horizontal deformations at IC1 and IC2 for section A1

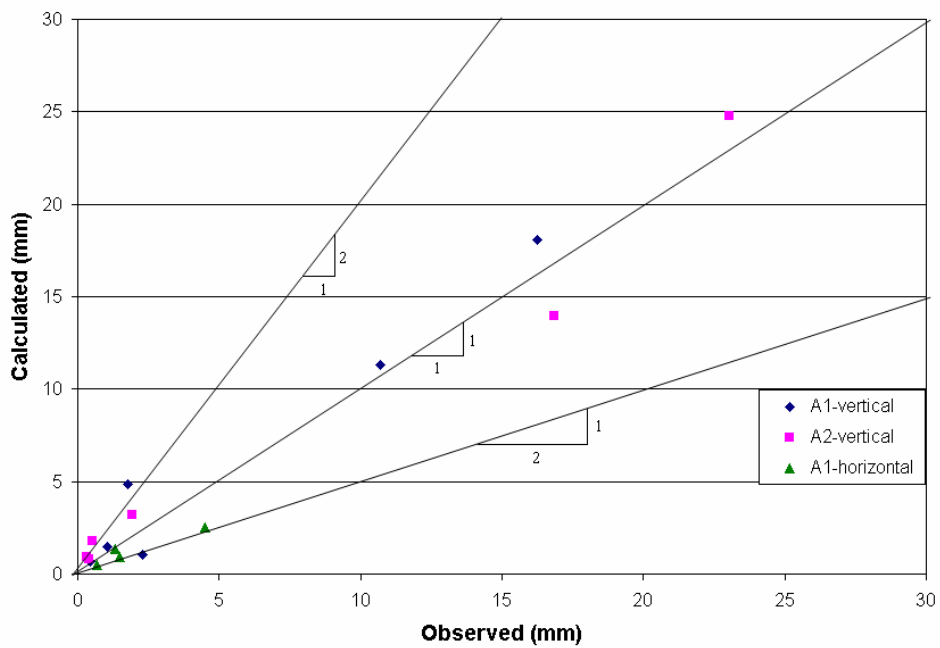


Figure 5.18: Observed and calculated displacements for EOC condition

5.3.4.3 Total Stresses

Total stresses in Muratlı Dam have been measured with the help of earthcells. As mentioned before, unit weights of the materials are calibrated with the help of the earthcell measurements. Locations of earthcells at section A1 are given in Figure 5.5.

All analyses are based on two dimensional assumption, as a result valley shape does not included in analyses. Stress reduction factors should be used to account for the valley shape. However, for Muratlı Dam both of the stress reduction factors are “1” since river width to height ratio is greater than 1.0 (Hunter and Fell, 2003). From Figure 5.5, it can be seen that earthcells are located at four different elevations; 64 m, 70 m, 80 m and 90 m. A comparison of observed and calculated values for section A1 is given in Table 5.9. In the table, it can be seen that the difference between observed and calculated values are significantly different for EC3, EC5, EC9, EC10, EC11 and EC14. Although EC9 and EC10 are located at same elevation with the same distance from the main dam axis but at opposite side of the axis, total pressures are observed to differ by a factor of about three for these earthcells. These values are expected to be close to each other as in the case for the analysis results. The same discussion is also valid for EC8 - EC11 and EC13 - EC14. A problem of connection system is considered to have caused a conflict. For example, the cables connecting EC3 and EC5 to the monitoring unit might have been mixed. In Figure 5.19 calculated and observed total stresses are shown for EOC. Almost all of the data fall in the region defined by lines with slopes 2:1 and 1:2.

Table 5.9: Comparison of total stresses for cross section A1

Inst.	Elevation (m)	X* (m)		Observed Values (kPa)	Calculated Values (kPa)	Difference (kPa)
		U.strm	D.strm			
EC1	64.41	77.00	-	215.20	159.78	55.42
EC2	64.36	71.00	-	197.32	174.18	23.14
EC3	64.56	42.00	-	522.70	374.40	148.30
EC4	64.85	16.00	-	530.68	531.11	0.43
EC5	63.98	6.02	-	360.79	557.23	196.44
EC6	64.00	-	6.00	539.35	560.54	21.19
EC7	64.35	-	19.38	464.58	499.53	34.95
EC8	70.19	16.56	-	387.79	441.45	53.66
EC9	70.04	6.47	-	663.51	474.95	188.56
EC10	69.95	-	7.55	229.06	466.55	237.49
EC11	69.76	-	20.08	236.87	408.64	171.77
EC12	80.07	16.47	-	220.41	283.43	63.02
EC13	80.17	6.44	-	274.93	322.55	47.62
EC14	80.24	-	6.41	136.44	314.66	178.22
EC15	80.19	-	19.28	281.68	239.89	41.79
EC16	89.94	6.20	-	140.96	171.53	30.57
EC17	90.02	-	6.29	92.13	156.09	63.96

*Distance to the main dam axis

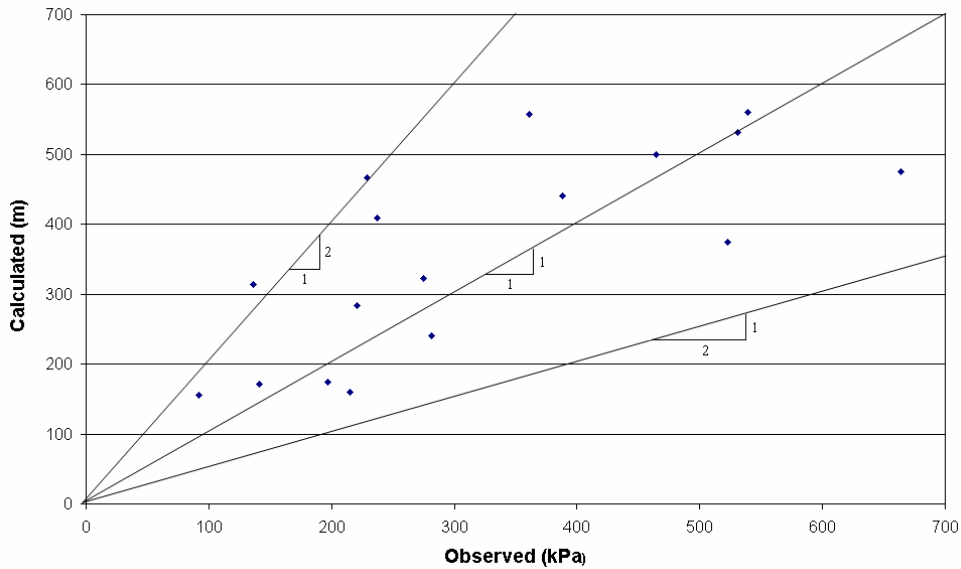


Figure 5.19: Observed and calculated total stresses for EOC condition

5.3.5 Reservoir Impoundment Analyses

Following the construction of an impervious faced rockfill dam, large deformations occur during first reservoir impoundment period since water load acts on the surface of the dam. A detailed explanation of these deformations is given in Chapter 4. Major part of the deformations due to reservoir filling occurs at upstream part of the body. Therefore, deformations that occur during this period affect the performance of the impervious face. Also, possible cracks which lead to leakage in the dam body may occur as a result of these deformations if the face can not tolerate the excessive deformation (Khalid et. al., 1990).

It has been studied by Saboya and Byrne (1993) that during reservoir impoundment, rockfill behaves stiffer compared to construction stage. Water loading causes an increase in minor and major principal stresses. The increase of minor principal stress is greater than the increase in major principal stress. As a result shear stress drops and unloading occurs. It can be said that initial filling of the reservoir causes a decrement in stress level in many elements. Therefore, measured deformations are smaller than expected. Deformation modulus of rockfill material is increased by a factor of two or three to obtain similar results as observed values. Continuing the filling of the reservoir causes an increment at stress level and elements revert back to a normal loading (Saboya and Byrne, 1993).

Filling the reservoir in Muratlı Dam was started at 14.03.2005 and continued up to the elevation of maximum operation level of 96 m. Although reservoir could have been filled in 10 days, it is raised stage by stage in a month to control the deformations.

In Plaxis analyses, reservoir impoundment condition is reflected as shown in Figure 5.20. Reservoir level is shown at its maximum elevation, 96 m. The phreatic line in the dam body and at downstream side is taken at the drainage pipe level since the impervious face prevents the flow in the dam body. Therefore, there is not any water flow in the dam body above the drainage pipe.

As mentioned previously, for reservoir impoundment condition rockfill material behaves stiffer than end of construction condition. This behavior is taken into account in hardening soil model by software, Plaxis v7.2 automatically. In these analyses, all the parameters are the same with the ones used for construction stage calculations except the deformation modulus which is taken as three times stiffer, as default of the program. Calculated and observed deformations after the reservoir impounding are compared to see the RI effect.

5.3.5.1 Vertical Deformations

A comparison of calculated results and observed values from the vertical fill-extensometers is summarized in Table 5.10. When the table is examined, although the agreement between the observed and calculated values is generally good at the locations of fill- extensometers; EW1, EW2 and EW15, the same can not be said for EW3, EW4 and EW9 where there exist significant differences between the measured and calculated values. It is suggested that the difference might be due to the unhomogeneity of the alluvium at those locations or due to calibration errors of the instruments.

Table 5.10: Comparison of calculated and observed vertical fill-extensometer values for RI

Inst.	Elevation (m)	Observed (mm)	Calculated (mm)	Difference (mm)
EW15	89.35-79.35	-2.00	-3.94	1.94
EW13	82.60-72.60	-	-14.41	-
EW9	74.89-64.89	-8.46	-31.08	22.62
EW4	71.00-64.00	-43.77	-16.39	27.38
EW3	71.00-64.00	-28.78	-16.83	11.95
EW2	61.50-51.50	-2.68	-1.63	1.05
EW1	61.07-51.07	-2.63	-2.97	0.34

Calculated settlements at location IC1 for section A1 are given in Figure 5.21. It can be seen from the figure that maximum settlement is about 5 mm. Settlements are relatively small since IC1 is located near the dam axis and this region of the dam body is not affected much from reservoir impoundment.

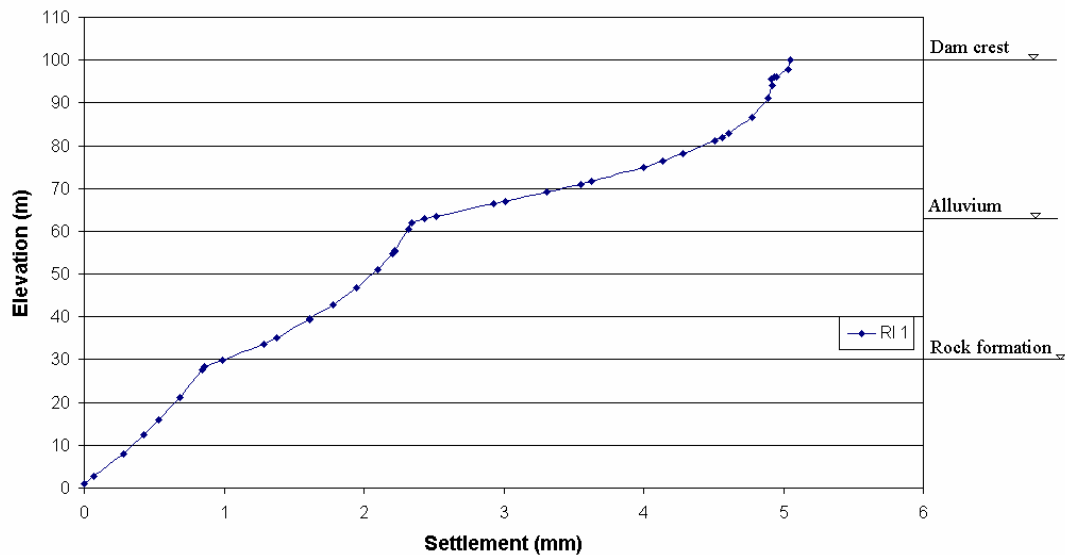


Figure 5.21: Calculated vertical deformations for reservoir impoundment

5.3.5.2 Horizontal Deformations

Observed measurements of horizontal fill-extensometers are also compared with calculated deformations. A comparison of calculated and observed values is given in Table 5.11. It may be said that analysis results are agreeable with the observed values at locations EW5 and EW16. However, there is a significant difference at the location EW14.

Calculated horizontal deformations at location IC1 are depicted in Figure 5.22. As it is mentioned before, results of analyses are not compared with measurements since those readings are not consistent and reliable. Maximum horizontal deformation is estimated to be about 3.5 mm, at location IC1.

In Figure 5.25 calculated and measured displacements for RI condition are given. It is seen that for the points in the dam body displacements scatter between the measurements and calculated values is larger.

Table 5.11: Comparison of calculated and observed horizontal fill-extensometer values for RI

Inst.	Elevation (mm)	Observed (mm)	Calculated (mm)	Difference (mm)
EW22	99.11	-	0.06	-
EW16	89.93	-0.71	-2.20	1.49
EW14	82.61	-2.94	-7.28	4.34
EW5	64.34	-1.13	-1.54	0.41

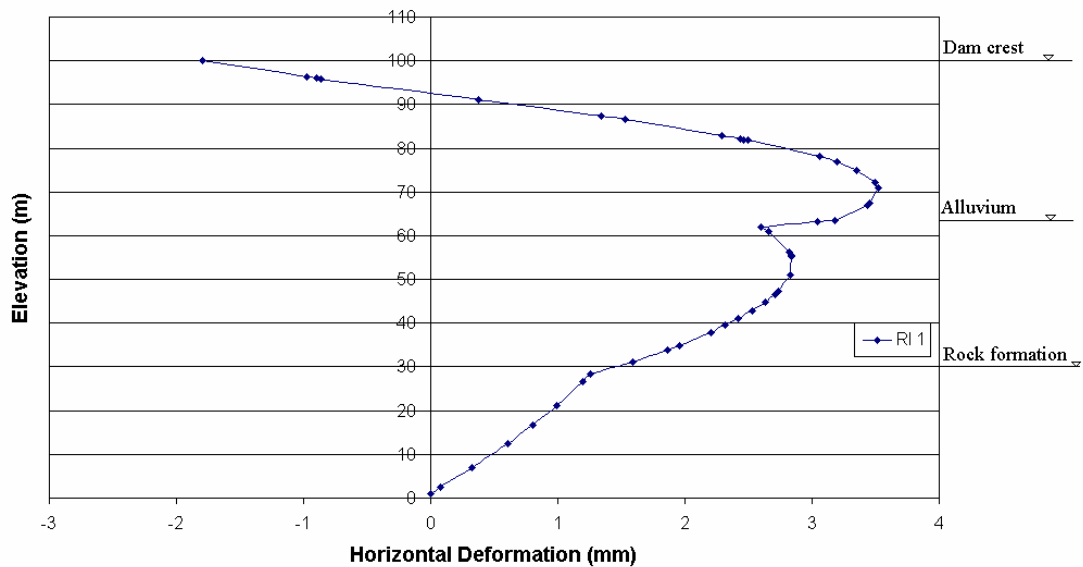


Figure 5.22: Calculated horizontal deformations for reservoir impoundment

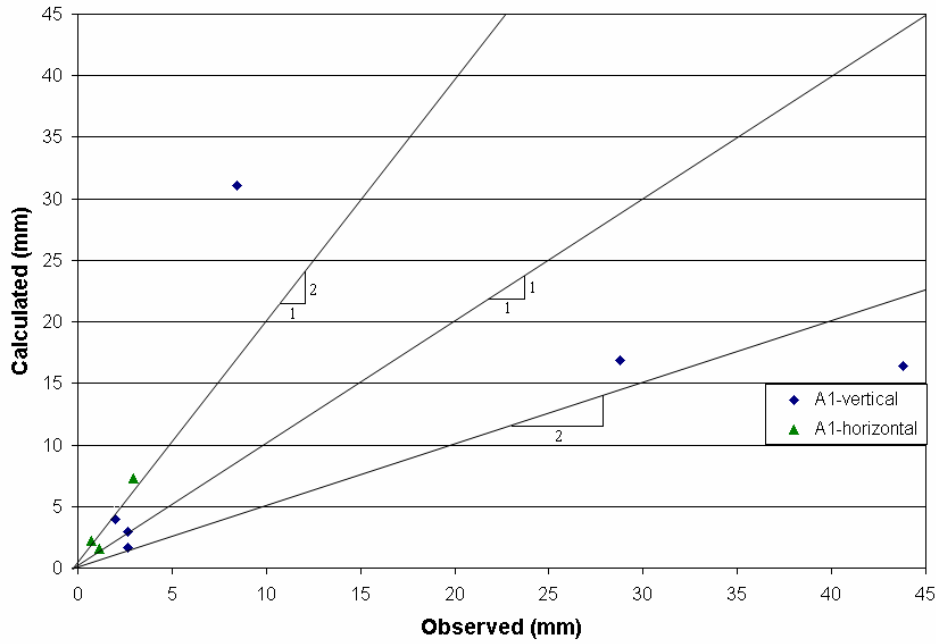


Figure 5.23: Observed and calculated displacements for RI condition

5.3.5.3 Total Stresses

Comparison of RI analysis results with earthcell measurements are presented in Table 5.12. Earthcells, EC3, EC4 and EC17 were reported to be failed during reservoir impoundment, which implies that data taken after reservoir impounding from these cells are unreliable. As it is pointed out before, there are calibration or construction errors at earthcells EC9, EC10, EC11 and EC14. Rest of the earthcells is in good agreement with the calculation results, as expected.

When Tables 5.9 and 5.12 are compared, it can be seen that total stresses increase with reservoir impoundment as a result of water load applied on the impervious face. The effect of the water load can be seen clearly at earthcells located at upstream region. However, this impact disappears towards the downstream region. For RI condition, calculated and observed stresses yield a better conformity than displacements, as depicted in Figure 5.24.

Table 5.12: Comparison of calculated and observed total stresses for RI

Inst.	Elevation (m)	X* (m)		Observed Values (kPa)	Calculated Values (kPa)	Difference (kPa)
		U.strm	D.strm			
EC1	64.41	77.00	-	401.20	393.08	8.12
EC2	64.36	71.00	-	301.00	303.27	2.27
EC5	63.98	6.02	-	367.55	595.86	228.31
EC6	64.00	-	6.00	566.76	574.54	7.78
EC7	64.35	-	19.38	472.15	504.69	32.54
EC8	70.19	16.56	-	424.58	487.53	62.95
EC9	70.04	6.47	-	676.75	498.40	178.35
EC10	69.95	-	7.55	234.73	474.00	239.27
EC11	69.76	-	20.08	241.50	407.03	165.53
EC12	80.07	16.47	-	230.05	312.81	82.76
EC13	80.17	6.44	-	275.28	333.14	57.86
EC14	80.24	-	6.41	134.77	316.28	181.51
EC15	80.19	-	19.28	280.44	241.61	38.83
EC16	89.94	6.20	-	139.25	177.40	38.15

*Distance to the main dam axis

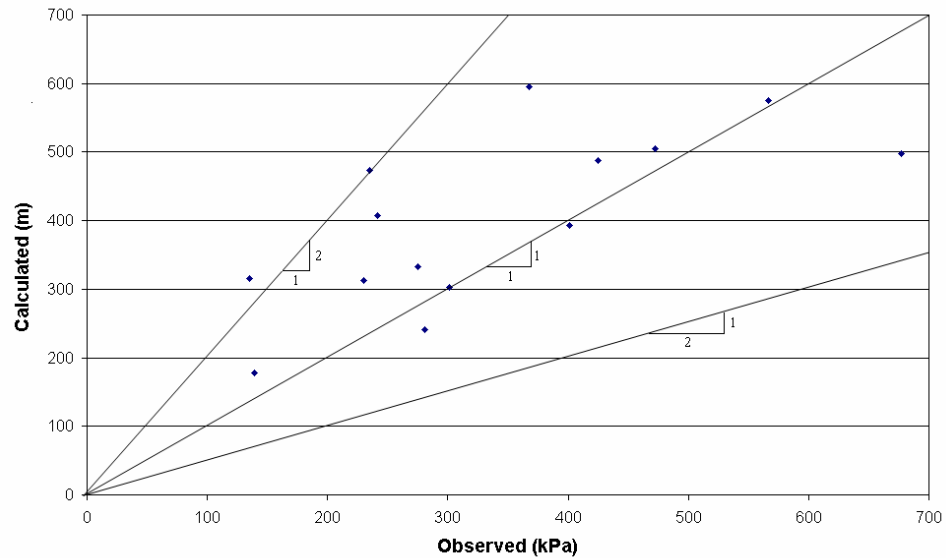


Figure 5.24: Observed and calculated total stresses for RI condition

5.3.6 Displacement and Stress Contours

Displacement and stress contours at section A1 are plotted for both end of construction and reservoir impoundment loading conditions. Figures from 5.25 to 5.29 and Figures from 5.30 to 5.34 depict end of construction and reservoir impoundment contours, respectively. For vertical and horizontal displacements negative values indicate settlement and upstream movement, respectively, where for stresses negative values indicate compression.

For the end of construction stage, the stresses and displacements in the upstream part is expected to be the mirror of downstream part (Khalid et. al., 1990). It is partially satisfied for horizontal, vertical and shear stresses and for vertical displacement contours. However, it can not be said for horizontal displacement contours.

From Figure 5.25, it can be seen that the movement at upper part of the dam is towards upstream direction and lower part of the dam and subsoil move towards downstream direction. A small downstream movement of cofferdam and a small upstream movement beneath the asphalt face are estimated. This behavior may be due to the unhomogeneity of the dam. Maximum horizontal displacements are 12.34 mm and 11.24 mm towards upstream and downstream directions, respectively.

When Figure 5.26 is examined, it can be seen that maximum settlement occurs at about mid-height of the dam as expected and its value is 106.07 mm. As it is mentioned above, the settlement of rockfill dams range between 0.25% and 1.00% of the dam height (Singh and Varshney, 1995). In Muratlı Dam, maximum settlement is calculated to be 0.29% of dam height for section A1 and 0.35% for section A2. It is also seen that, calculated horizontal displacements are smaller than vertical displacements.

For EOC condition, maximum horizontal and vertical stresses are 981.58 kPa and 1973.69 kPa, respectively (Figure 5.27 and Figure 5.28). When horizontal and

vertical stress contours are examined, it can be seen that stress contours has a peak at the centerline of the dam and they decrease towards the faces at the same elevation. From Figure 5.29, it can be seen that the shear stresses at dam axes are zero and increase significantly towards the faces. Maximum shear stresses at upstream and downstream regions are 142.44 kPa and 92.60 kPa, respectively.

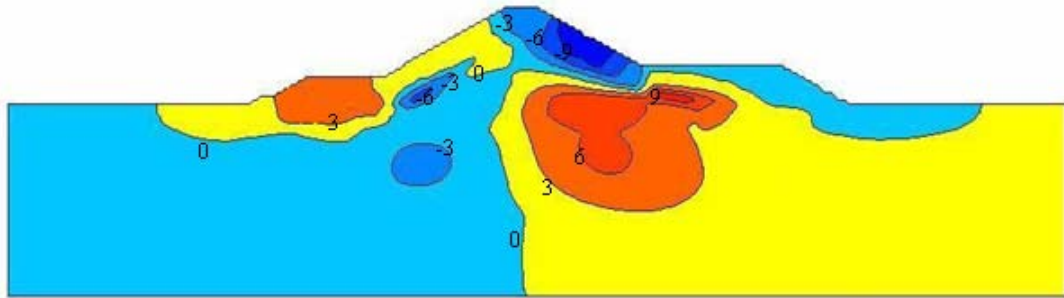


Figure 5.25: Horizontal displacements for EOC (in mm)

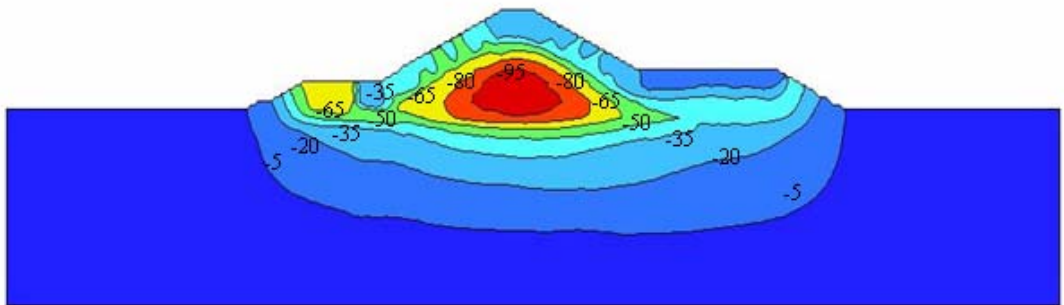


Figure 5.26: Vertical displacements for EOC (in mm)

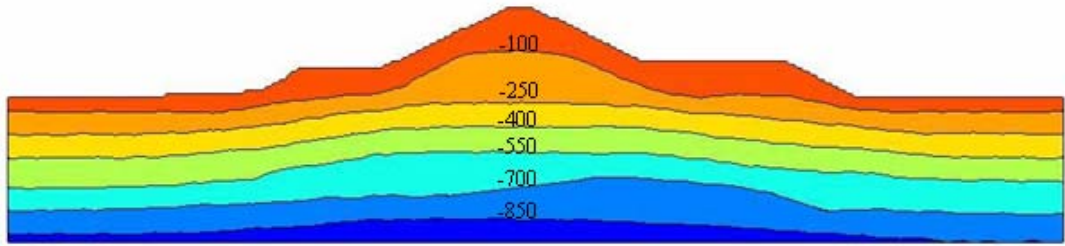


Figure 5.27: Horizontal stresses for EOC (in kPa)

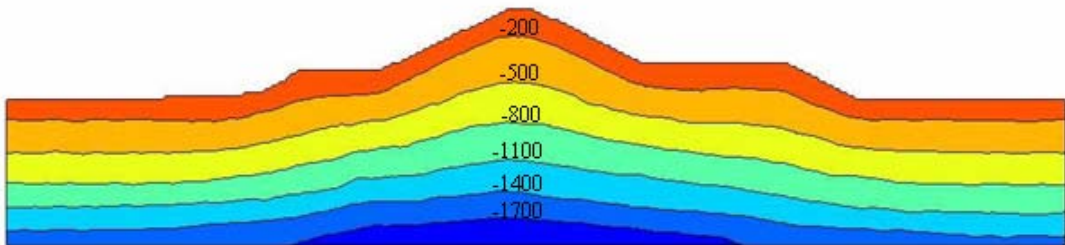


Figure 5.28: Vertical stresses for EOC (in kPa)

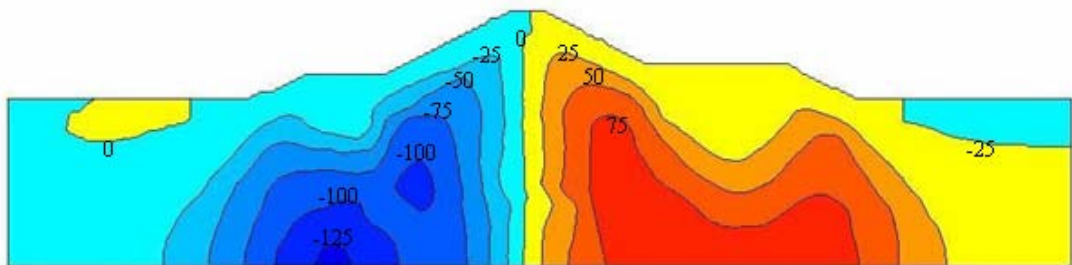


Figure 5.29: Shear stresses for EOC (in kPa)

Maximum water level is taken as 96 m for impoundment condition. When horizontal displacements at RI condition are considered, it is seen that, the whole dam body and a part of the subsoil move towards downstream, as expected. Horizontal displacements are concentrated at upstream face and they decrease towards the downstream. Maximum horizontal displacement is 49.48 mm near the cutoff wall (Figure 5.30).

Water load causes vertical displacement of the upstream face. Downstream half of the dam body is not significantly affected from impounding. Maximum vertical displacement is 69.31 mm near the cutoff wall (Figure 5.31).

When horizontal and vertical stress contours for RI condition are compared with contours for EOC, it is observed that stress increments due to water load do not affect the downstream part much. However stress increment at upstream half is considerable. Maximum horizontal stress reaches to 1270.63 kPa and maximum vertical stress is found to be 2060.06 kPa, both of which occur at the base (Figures 5.32-5.33).

When reservoir is filled with water, water load pushes the dam body towards the downstream direction as shown in Figure 5.34. As a result, negative shear stresses at upstream decrease considerably and positive shear stresses at downstream significantly increase. Also, it is observed that shear stress increments are concentrated near the dam axis. Maximum negative shear stress becomes 49.02 kPa at upstream and maximum positive shear stress becomes 255.29 kPa for the downstream.

In general, calculated stress and displacement patterns obtained for Muratlı Dam, both for end of construction and reservoir impoundment loading cases indicate a general agreement with results of studies for Cethana Dam (Khalid et. al.,1990) and Kürtün Dam (Özkuzukıran et. al., 2006).

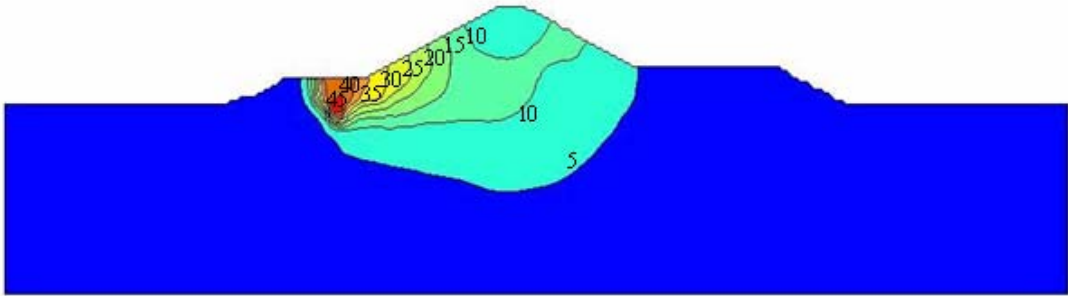


Figure 5.30: Horizontal displacements for RI (in mm)

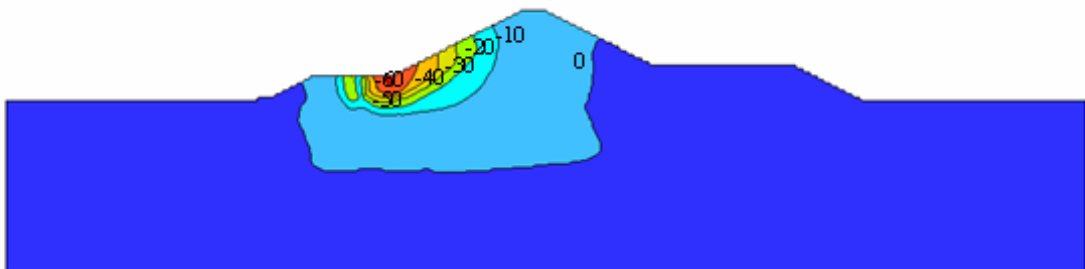


Figure 5.31: Vertical displacements for RI (in mm)

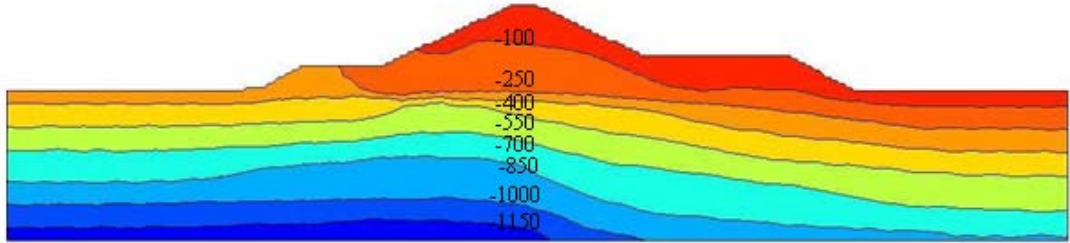


Figure 5.32: Horizontal stresses for RI (in kPa)

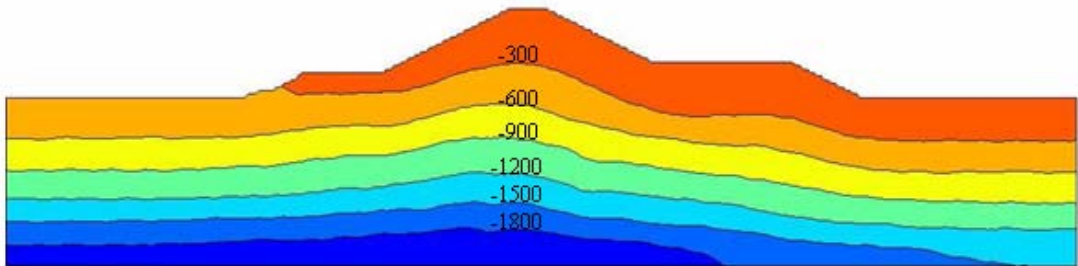


Figure 5.33: Vertical stresses for RI (in kPa)

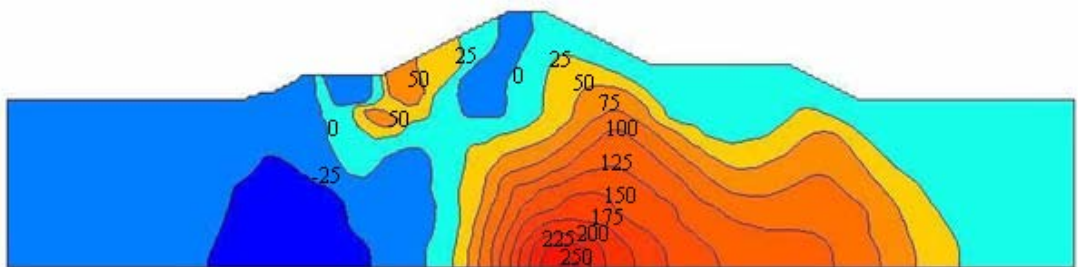


Figure 5.34: Shear stresses for RI (in kPa)

5.4 Pore Pressure in Muratlı Dam:

The piezometers at Muratlı Dam are installed to check the effectiveness of the cutoff wall. Piezometers at the dam are located at upstream and downstream side of cutoff wall in the alluvium and transition zone. Variation of total head measurements versus time for two piezometers located at cross section A1 is shown in Figure 5.35. In the same figure, change of fill level and reservoir water with time is depicted. A1PW5 and A1PW6 are located at the upstream and downstream sides of the cutoff wall, having the same elevation. From the figure, the effect of the cutoff wall is seen clearly. Although the total head observed at A1PW5 follow the same pattern with the reservoir level, total head at A1PW6 is not affected much from reservoir filling, as expected.

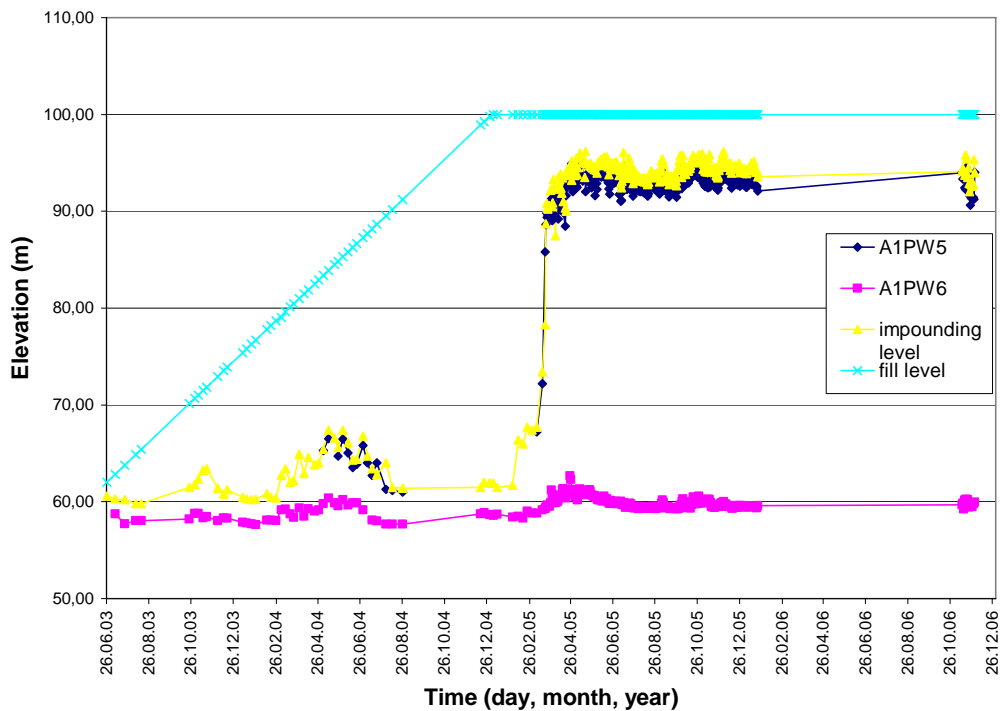


Figure 5.35: Total head measurements for Muratlı Dam

Two dimensional steady-state seepage analyses are performed to compare the observed and calculated pore pressures. Seep-W software is used to analyze the dam for both end of construction and reservoir full conditions. All the materials used in the model are assumed to have constant coefficient of permeability. Materials used in the model are given in Table 5.13 with their coefficient of permeability values (Values are taken from Verbundplan Final Design Report of Muratlı Dam, 2001). Filter material, riprap are assumed as alluvium fill since their coefficient of permeabilities are almost the same. Also it is assumed that coefficient of permeability for all materials do not change with the direction which means the ratio of the k_y (vertical coefficient of permeability) to k_x (horizontal coefficient of permeability) is 1.0.

Table 5.13: Coefficient of permeability values for Murath Dam

Material	Zone	Coefficient of Permeability (m/s)
Rockfill	3A, 3B, 3C	1.0E-2
Alluvium fill	1, 2A, 2B, 5, 6	1.0E-4
Subsoil	-	1.0E-4
Rock	-	8.0E-6
Cutoff	-	1.0E-7
Asphalt face	7	1.0E-8
Core cofferdam	4	1.0E-7
Drainage	-	1.0E-1

Mesh for the dam, formed with nine-noded quadrilateral elements and three-noded triangular elements in transition zones, is given in Figure 5.36. Boundary conditions are defined in terms of total head and total flux. For end of construction, upstream total head is observed to be 67.70 m and downstream total head to be 58.90 m. When full reservoir condition is considered, upstream total head becomes 96.00 m and downstream total head becomes 61.20 m. Total flux is zero across the left and right vertical boundaries and across the bottom of the finite element mesh for both conditions.

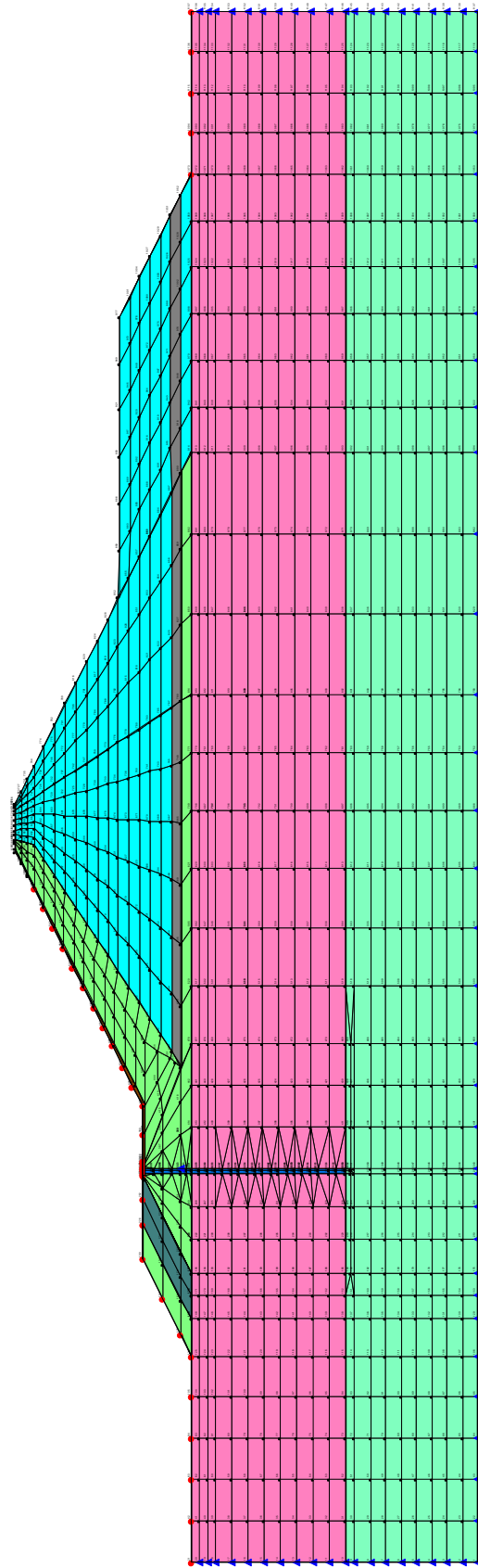


Figure 5.36: Finite element mesh used in the seepage analyses

Figure 5.37 and 5.40 shows the velocity vectors corresponding to end of construction and reservoir full conditions, respectively. It can be seen that leakage from cutoff wall follows drainage pipe pattern. Pore pressure distribution and total head distribution for EOC are given in Figure 5.38 and Figure 5.39, respectively. Both of them decrease towards the downstream side of the cutoff wall. Total head beneath the cutoff wall is between 62-64 m.

As mentioned before, for reservoir impoundment condition, max water level is 96 m. Reservoir level is increased from 67.70 m to 96.00 m in a month. Figure 5.41 and Figure 5.42 show pore pressure distribution and total head distribution for RI condition, respectively. Both of them decrease from upstream to downstream side due to cutoff wall. Total head beneath the cutoff wall is between 78-82 m.

The effect of cutoff wall for RI case can be seen clearly in Figure 5.43. It can easily be seen that total head decreases from 96 m to 61 m at the location of cutoff wall. A comparison of calculated and observed total heads is presented in Table 5.14. The locations of the piezometers at cross section A1 can be seen in Figure 5.5. In general, calculated total heads are in a good agreement with observed total heads. PW12, PW17, PW22 and PW23 are not considered for both of the conditions since observed measurements are unreliable. Also, there may be a calibration error at PW10. For EOC case, calculated heads are about 3-4 m smaller than observed heads at piezometers which are located in alluvial fill (PW8, PW9, PW16, PW18, PW19, PW20 and PW21). This may be due to the pore pressure increments during the compaction of the alluvium containing some fine materials. However, for RI condition calculated total heads at these piezometers are very close to measurements.

A plot for measured pore pressures versus predicted ones exhibit a good agreement as can be seen from Figure 5.44.

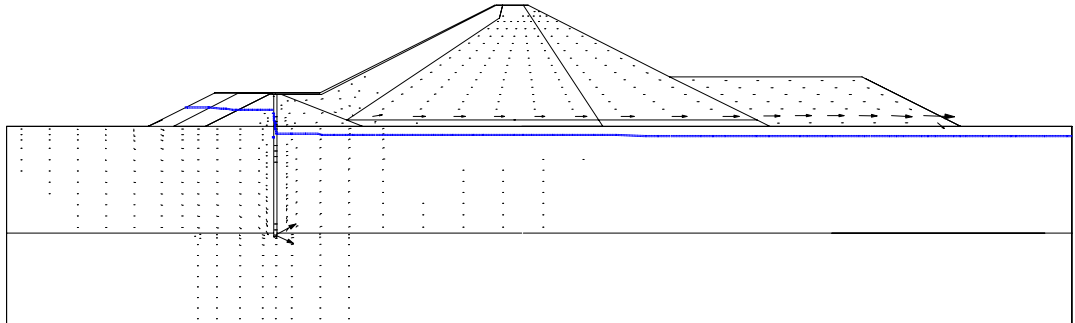


Figure 5.37: Velocity vectors for EOC (magnified 2.5e+5)

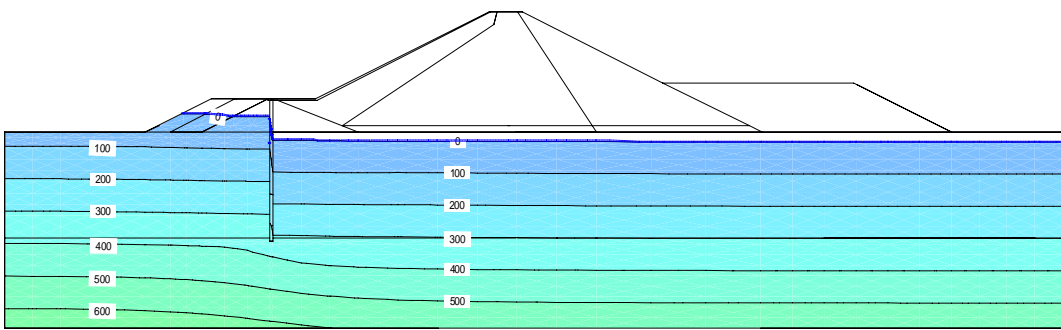


Figure 5.38: Pore pressure distribution for EOC

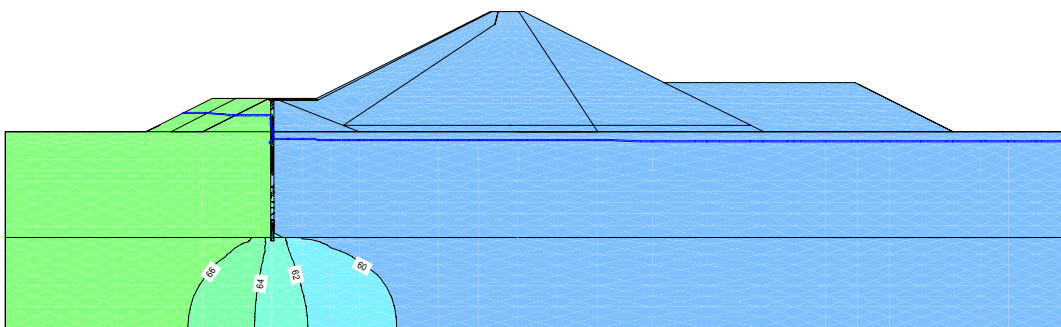


Figure 5.39: Total head distribution for EOC

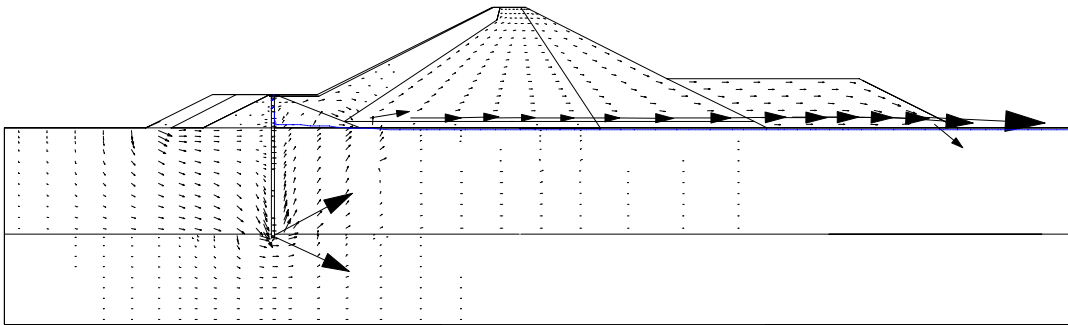


Figure 5.40: Velocity vectors for RI (magnified $2.5e+5$)

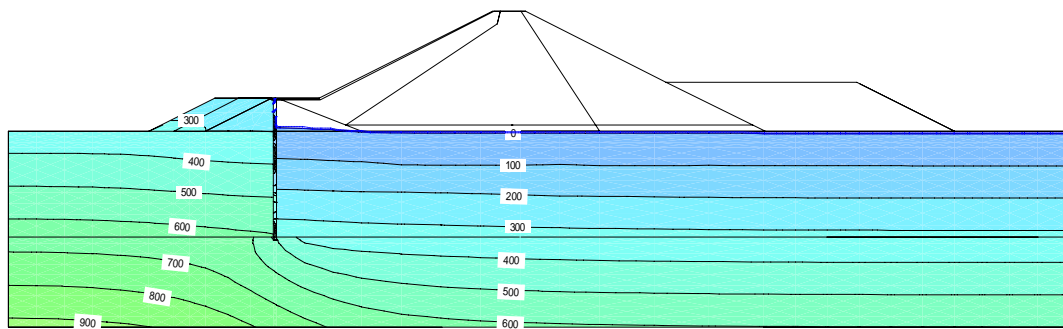


Figure 5.41: Pore pressure distribution for RI

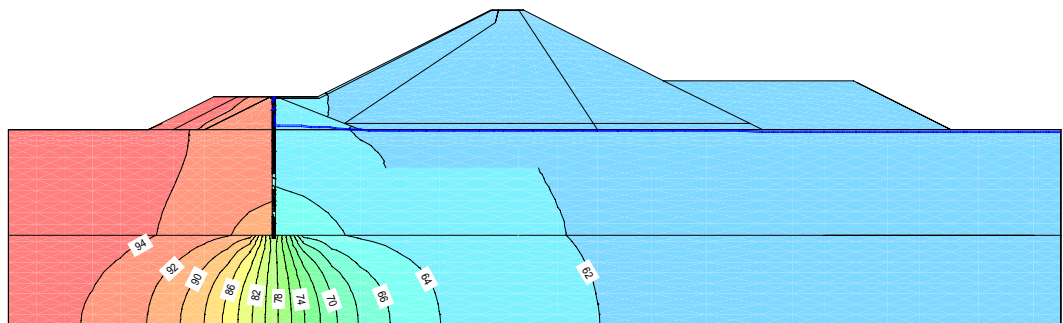


Figure 5.42: Total head distribution for RI

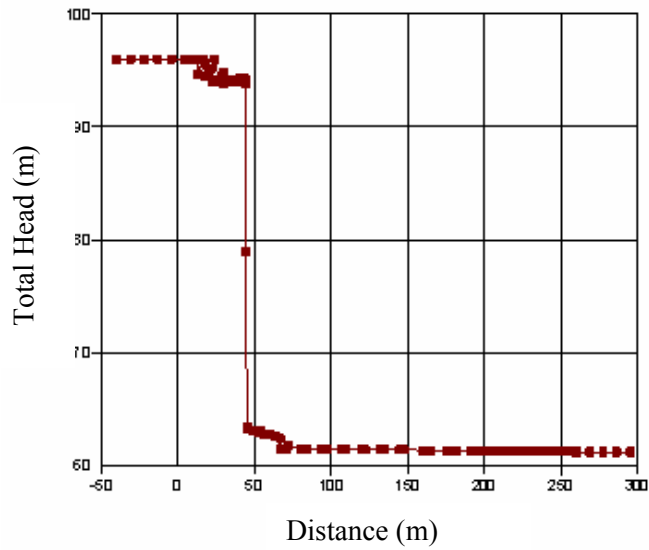


Figure 5.43: Total head versus distance graph for RI

Table 5.14: Comparison of calculated and observed total heads

Inst.	Elevation (m)	EOC		RI	
		Obs. (m)	Calc. (m)	Obs. (m)	Calc. (m)
PW1	30.00	65.71	66.52	93.78	91.84
PW2	30.00	55.74	59.86	63.04	65.14
PW3	40.00	-	66.74	93.60	92.79
PW4	40.00	57.87	59.63	62.42	64.22
PW5	50.00	67.19	66.85	94.62	93.35
PW6	50.00	58.82	59.47	61.33	63.58
PW7	64.50	67.56	66.85	93.22	94.01
PW8	64.50	63.66	59.35	64.01	63.13
PW9	69.50	69.99	66.82	94.58	94.16
PW10	69.50	69.60	59.33	74.79	63.09
PW11	59.50	58.56	59.07	62.06	61.93
PW13	58.00	58.11	58.94	58.58	61.39
PW14	58.00	58.64	58.97	60.61	61.48
PW15	57.00	58.56	58.94	60.73	61.38
PW16	64.50	63.62	58.95	63.53	61.42
PW18	64.00	62.52	58.94	62.74	61.39
PW19	64.00	63.17	58.94	63.17	61.39
PW20	64.50	63.31	58.94	63.56	61.38
PW21	62.00	61.36	58.94	61.27	61.36

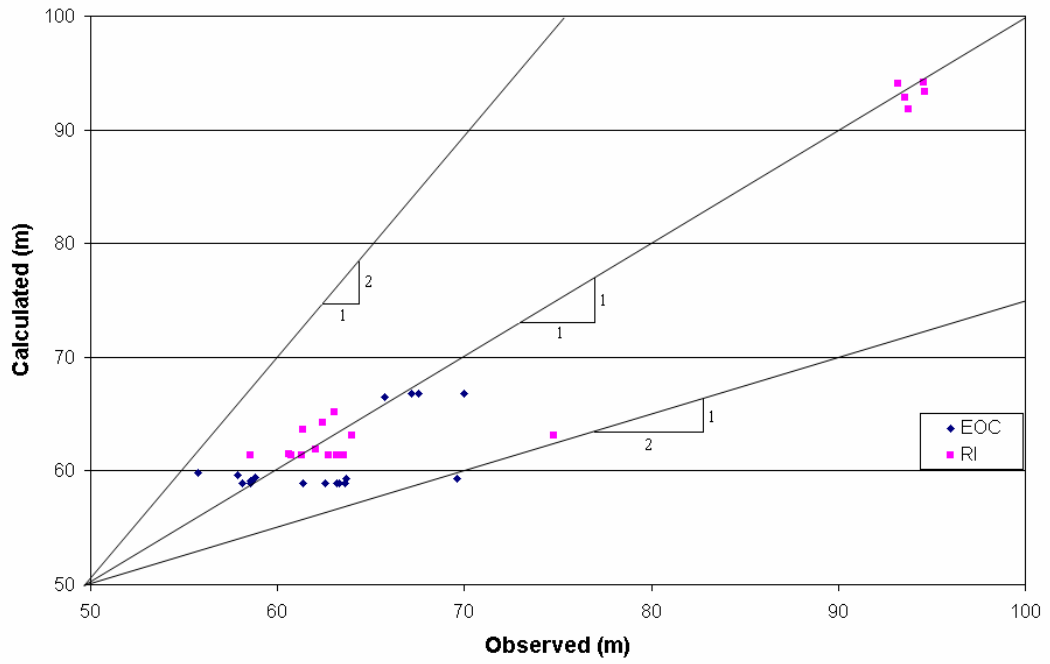


Figure 5.44: Observed and calculated total heads for EOC and RI conditions

CHAPTER 6

CONCLUSION

In this study, deformation behavior of Muratlı Dam, the first asphalt faced rockfill dam in Turkey is investigated by two dimensional finite element method. Finite element program Plaxis v7.2 is used in calculating the displacements and stresses. Nonlinear, stress dependent and inelastic behavior of the fill materials are incorporated into the hardening soil model to assess the displacements and stresses which are compared with the measured values for both end of construction (EOC) and reservoir impoundment (RI) conditions. The steady-state flow through the permeable foundation of the dam with an impervious cutoff wall is also studied by software Seep-W and total heads are compared with measured values. The major conclusions drawn from this study are summarized as follows:

- Noting, calculated vertical and horizontal displacements are compared with fill-extensometer measurements since inclinometer measurements are not reliable, calculated displacements are found to be larger than fill-extensometer measurements. Nevertheless, overall agreement is quite encouraging: measured and calculated displacements are both at the same order of magnitude. The differences between calculated and observed displacements may be due to certain variations in compaction energy applied during construction.
- For EOC analyses, maximum vertical displacement is 109 mm (0.29% of height of the dam, H) and 146 mm (0.35% of H) for cross sections A1 and A2 at the end of construction, respectively. The location of the maximum vertical displacement is about mid-height of the dam body for both of the sections as expected.

- When horizontal displacement contours for EOC condition are examined, it is seen that upper half of downstream part moves towards upstream, whereas lower half of the dam body and subsoil move towards downstream. The similar behavior is also observed at the upstream part. This may be due to the unhomogeneity of the dam. The behavior of the horizontal displacements shows similarity with the study of Özkuzukıran et. al. (2006). A comparison of measured and calculated horizontal displacements could not be made since horizontal displacements were not measured through out the dam body, except at a few locations near the surface.
- During impoundment of the reservoir, rockfill behaves much stiffer than during construction due to the fact that water load on the impervious face causes unloading effect in the dam body. This unloading behavior can be simulated by hardening soil model. A comparison of observed displacements with calculated ones considering an unloading modulus is agreeable.
- For reservoir impoundment case maximum vertical displacement occurs under impervious face and is about 69 mm (this value does not include the EOC displacements). Downstream region of the dam is not affected much from reservoir impoundment. Behavior of the dam in terms of horizontal and vertical displacements is consistent with the previous studies.
- Calculated and measured stresses are generally close to each other, for both EOC and RI conditions except for some of earthcell readings. It may be noted for these instruments, the measured values are not consistent with the requirements for vertical equilibrium. No stress reduction factors are used to account for the effect of abutments, since they are not steep.
- Horizontal and vertical stress contours increase gradually going from the crest of the dam to base. Stresses are mirrored approximately at upstream and downstream parts. When RI condition is considered, behavior of the stresses is similar to that of EOC condition, but the values of the stresses are larger. These stress increments are significant in upstream region and negligible in downstream region.

- When shear stresses are examined, the shear stress at the main dam axis is zero and they increase significantly through the upstream and downstream halves for EOC, and stresses are larger at upstream half. For RI, water load pushes the dam body towards downstream. Therefore, negative shear stresses at upstream part decrease and positive shears at downstream part increase. The behavior is in concordance with the previous studies.
- When piezometer measurements are considered, it is seen that total heads significantly decrease towards downstream indicating that cutoff wall works satisfactorily. Piezometers located at upstream side of the cutoff wall follow the reservoir level, whereas piezometers at downstream side are not affected much from reservoir filling.
- A comparison of calculated total heads with the observed ones indicates a general agreement. However, for EOC condition there is a significant difference at some piezometers located in alluvial fill. It is suggested that, this difference may be due to the high fine contents in the compacted fill.

It can be said that two dimensional finite element analyses can be used to predict displacements and stresses with a reasonable accuracy. Analyses results may be used to understand the behavior of the dam at locations where no instruments are installed.

The study indicates that the locations of the displacement and stress measuring instruments are generally suitable for the purpose. Maximum displacement values found at the dam center is not compared with the related instrument readings since inclinometers placed here are not operated properly. Therefore, maintenance of instruments during and after the construction is a vital issue.

For further studies, a 3-D analysis can be carried out to understand the effect of the third dimension. On the other hand, an analysis of transient seepage is suggested to assess the change of total head in time.

REFERENCES

1. Bodtman, W. L., and Wyatt, J. D., 1985. "Design and Performance of Shiroro Rockfill Dam", Proc. of the Symp. "Concrete Face Rockfill Dams: Design, Construction and Performance", ASCE, 231-251.
2. Clough, R. W., and Woodward, R. J., 1967. "Analysis of Embankment Stresses and Deformations", J. of Soil Mech. and Found. Div., ASCE, 93, SM4, 529-549.
3. Cooke, J. B., 1984. "Progress in Rockfill Dams", (18th Terzaghi Lecture), J. Geotech. Engrg., ASCE, 110, 10, 1381-1414.
4. Cooke, J. B., and Sherard, J. L., 1987. "Concrete-Face Rockfill Dam: I. Assessment", J. Geotech. Engrg., ASCE, 113, 10, 1096-1112.
5. Cooke, J. B., and Sherard, J. L., 1987. "Concrete-Face Rockfill Dam: II. Design", J. Geotech. Engrg., ASCE, 113, 10, 1113-1132.
6. Dascal, O., 1987. "Postconstruction Deformations of Rockfill Dams", J. Geotech. Engrg., ASCE, 113, 1, 46-59.
7. Duncan, J. M., and Chang, C. Y., 1970. "Nonlinear Analysis of Stress and Strain in Soil", J. of Soil Mech. and Found. Div., ASCE, 96, SM5, 1629-1653.
8. Fitzpatrick, M. D., Cole, B. A., Kinstler, F. L., and Knoop, B. P., 1985. "Design of Concrete-Faced Rockfill Dams", Proc. of the Symp. "Concrete Face Rockfill Dams: Design, Construction, and Performance", ASCE, 410-434.
9. Fumagalli, E., 1969. "Tests on Cohesionless Materials for Rockfill Dams", J. of Soil Mech. and Found. Div., ASCE, 95, SM1, 313-332.

10. Hunter, G., and Fell, R., 2003. "Rockfill Modulus and Settlement of Concrete Face Rockfill Dams", *J. Geotech. Geoenv. Engrg.*, ASCE, 129, 10, 909-917.
11. Janbu, N., 1963. "Soil Compressibility as Determined by Oedometer and Triaxial Tests", *Proc. of the European Conf. on Soil Mech. and Found. Engrg.*, Germany, vol.1, 19-25.
12. Kalkani, E. C., and Michali, A. J., 1984. "Steady Flow Calculations for Cutoff Wall Depth Variation", *J. Geotech. Engrg.*, ASCE, 110, 7, 899-907.
13. Khalid, S., Singh, B., Nayak, G. C., and Jain, O. P., 1990. "Nonlinear Analysis of Concrete Face Rockfill Dam", *J. Geotech. Engrg.*, ASCE, 116, 5, 822-837.
14. Kondner, R. L., 1963. "Hyperbolic Stress-Strain Response. Cohesive Soils", *J. of Soil Mech. and Found. Div.*, ASCE, 89, SM1, 115-143.
15. Kulhawy, F. H., and Duncan, J. M., 1972. "Stresses and Movements in Oroville Dam", *J. of Soil Mech. and Found. Div.*, ASCE, 98, SM7, 653-665.
16. Lefebvre, G., Duncan, J. M., and Wilson, E. L., 1973. "Three-Dimensional Finite Element Analysis of Dams", *J. of Soil Mech. and Found. Div.*, ASCE, 99, SM7, 495-507.
17. Leps, T. M., 1970. "Review of Shearing Strength of Rockfill", *J. of Soil Mech. and Found. Div.*, ASCE, 96, SM4, 1159-1170.
18. Lollino, P., Cotecchia, F., Zdravkovic, L., and Potts, D. M., 2005. "Numerical Analysis and Monitoring of Pappadai Dam", *Can. Geotech. J.*, 42, 1631-1643.
19. Nobari, E. S., and Duncan, J. M., 1972. "Movements in Dams due to Reservoir Filling", *ASCE: Specialty Conf. On Performance of Earth and Earth Supported Structures*, 797-815.

20. Özkuzukıran, S., Özkan, M. Y., Özyazıcıoğlu, M., and Yıldız, G. S., 2006. "Settlement Behavior of a Concrete Faced Rock-fill Dam", *Geotech. and Geolog. Engrg. J.*, 24, 6, 1665-1678.
21. Pagano, L., Sica, S., and Desideri, A., 2006. "Representativeness of Measurements in the Interpretation of Earth Dam Behavior", *Can. Geotech. J.*, 43, 87-99.
22. Plaxis v. 7.2 - Material Models Manual, 2004.
23. RocTest Telemac Instrumentation Manual, 2000.
24. Saboya, F. Jr., and Byrne, P. M., 1993. "Parameters for Stress and Deformation Analysis of Rockfill Dams", *Can. Geotech. J.*, 30, 690-701.
25. Schanz, T., Vermeer, P. A., and Bonnier, P. G., 1999. "The Hardening Soil Model: Formulation and Verification", *Beyond 2000 in Computational Geotechnics-10 Years of Plaxis*, Balkema, Rotterdam.
26. Seep-W v5.0 - User's Guide Manual, 2004.
27. Singh, B., and Varshney, R. S., 1995. "Engineering For Embankment Dams", A.A. Balkema Publishers, Brookfield.
28. Szostak-Chrzanowski, A., and Massiera, M., 2006. "Relation between Monitoring and Design Aspects of Large Earth Dams", *Proc. of 12th Int. FIG Symp. on Deformation Measurements and Analysis*, Baden.
29. Verbundplan Final Design Review Report, 2001.
30. Xing, H., Gong, X., Zhou, X., and Fu, H., 2006. "Construction of Concrete-Faced Rockfill Dams with Weak Rocks", *J. Geotech. Geoenv. Engrg., ASCE*, 132, 6, 778-785.